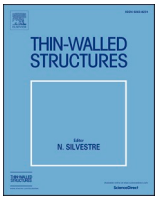
Thin–Walled Structures 216 (2025) 113719



Contents lists available at ScienceDirect

Thin-Walled Structures

journal homepage: www.elsevier.com/locate/tws





Effect of combined high temperature and tensile load on the post-fire performance of high-strength steel

A. Lapuebla-Ferri [a], D. Pons [a], M.L. Romero [a,b,*], L. Gardner [c]

[a] Department of Continuum Mechanics and Theory of Structures. Universitat Politècnica de València. Camí de Vera, s/n. 46022 València, Spain
[b] ICITECH. Universitat Politècnica de València, Valencia, Spain
[c] Imperial College London, London, United Kingdom

ARTICLE INFO

Keywords:
Carbon steel
Eurocode 3
Experiments, High-strength steel
Post-fire behaviour
Production route
Residual properties

ABSTRACT

An experimental campaign to evaluate the post-fire performance of grade S700 steel specimens subjected to a range of temperatures between 300 °C and 1000 °C and simultaneous tensile load, followed by natural cooling to room temperature, has been undertaken and is presented herein. The adopted test procedure provides a close representation of real fire and post-fire scenarios, since during a fire a structure is also subjected to a certain load level, an aspect that is usually neglected in research on this topic. The residual values of the key mechanical properties, including the yield strength, ultimate strength, Young's modulus, strain at fracture and ultimate strain, were computed. According to the experimental results, the post-fire response was found to be dependent on the production route of the tested material and, under some combinations of temperature and tensile load, the residual values of ultimate strain did not meet the Eurocode 3 ductility requirements, indicating that the residual ductility of a steel structure surviving a fire could be compromised. The present work provides valuable data for the safety assessment of structures after fires, and aids decision-making on whether to re-use, retrofit or demolish.

1. Introduction

High-strength steel (HSS) is a high-performance family of structural steels with a yield strength higher than 460 MPa. Among another advantages, HSS has a superior strength-to-weight ratio, so lighter structural elements can be manufactured compared to the use of conventional steels [1–3]. This feature leads to cost savings in transportation and erection, as well as environmental benefits due to reduced embodied carbon, thus positively impacting sustainability. Consequently, HSS has become increasingly suited to diverse structural engineering applications [4], so its application in structural engineering has increased significantly in recent decades.

In spite of this, the performance HSS in fire conditions is a topic of particular concern [5–9], given the deterioration of the mechanical properties of structural steel at elevated temperatures. Fire design aims to ensure that structures retain sufficient load-bearing capacity to allow the safe evacuation of the occupants and facilitate the firefighting operations. Achieving this goal requires a thorough understanding of the mechanical and thermal properties of steel at elevated temperatures. Fire incidents in steel-framed buildings, such as those in the World Trade Center (New York, USA, 2001), Parque Central (Caracas, Venezuela, 2004) and Windsor Tower (Madrid, Spain, 2005) are reminders that further research on this topic is needed.

In a number of previous experimental studies, the elevated temperature mechanical properties of HSS have been investigated through two primary testing methodologies: isothermal (steady-state tests) and anisothermal (transient-state tests). In steady-state tests, specimens are heated to a constant temperature before straining to failure [10–17], while transient-state tests involve applying tensile stress to a specimen and subsequently increasing temperature at a constant rate until failure occurs. Although steady-state tests are easier to perform, transient-state tests are more representative of real fire conditions, so both modes of testing are often performed [18–23]. In addition, research has also addressed the thermal properties of steel, including thermal expansion, specific heat and thermal conductivity [24]. The above studies have provided essential data for the design and safety assessment of steel structures under fire conditions.

Despite growing knowledge of the behaviour of HSS at elevated temperatures, research on its post-fire response remains relatively

* Corresponding author at: Department of Continuum Mechanics and Theory of Structures. Universitat Politècnica de València. Camí de Vera, s/n. 46022 València, Spain.
E-mail address: mromero@mes.upv.es (M.L. Romero).

https://doi.org/10.1016/j.tws.2025.113719
Received 24 April 2025; Received in revised form 29 June 2025; Accepted 13 July 2025
Available online 14 July 2025
0263-8231/Crown Copyright © 2025 Published by Elsevier Ltd. This is an open access article under the CC BY-NC-ND license (http://creativecommons.org/licenses/by-nc-nd/4.0/).

Notation

f_y	yield strength (0.2% proof strength).
f_u	ultimate strength.
t	specimen thickness.
t_s	soaking time.
E	Young's modulus.
$E_{fi,d}$	design effect of an action in the fire situation.
$R_{fi,d,0}$	design value of the member resistance in the fire situation at the onset of the fire.
ε_f	strain at fracture.
ε_u	ultimate strain.
ε_y	yield strain.
θ_0	room temperature.
θ_{crit}	critical temperature.
θ_t	target temperature.
σ_t	target tensile stress in transient-state and post-fire (loaded) tests.
μ_0	degree of utilisation.

However, this is not a reliable indicator of the residual properties of steel.

To accurately assess if a HSS structure can be safely reinstated after a fire, the residual mechanical properties of the steel must fulfil the provisions of the current structural design codes, or account should be taken for reduced reliability resulting from fire damage [29]. In either case, extensive experimental data on the mechanical performance of HSS after a fire is required.

Recent studies have started addressing this gap by examining the post-fire performance of HSS [30–36]. The findings show that the post-fire mechanical behaviour of HSS is dependent on a number of factors, such as the steel grade, the production route, the peak temperature reached during the fire and the method (and associated rate) of cooling. However, in many of these experiments, the test specimens remained unloaded while being subjected to a cycle of heating and cooling. Although this is a straightforward approach, it does not accurately replicate the real situation of a structure during a fire since, in reality, the load-bearing elements are subjected to loading throughout the entire duration of the fire, even if the building has been evacuated.

Relatively few experimental studies have examined the combined effect of load and elevated temperature on the post-fire performance of HSS [37]. In existing studies examining the combination of load and high temperature on steel reinforcing bars [38], it was shown that residual mechanical properties, particularly ductility, may fail to meet the requirements of Eurocode 3 [39] after experiencing certain load-temperature conditions.



Fig. 1. Experimental test setup. 1: upper block. 2: lower block. 3: electric furnace. 4: extensometer.

Table 1
Chemical composition of the steel grades tested in this work (weight %).

Steel grade	C	Si	Mn	Ni	Cr	Cu	Mo	Al	Ti	Nb	V	B
S355	0.180	0.23	1.53	0.28	0.29	0.30	0.18	0.034	0.02	0.045	0.011	–
S700	0.059	0.01	1.85	0.04	0.04	0.02	0.10	0.056	0.10	0.059	0.012	0.0002

limited. Knowledge of the residual properties of HSS after a fire is crucial in evaluating the condition of a structure after a fire and in determining whether the structure can be reinstated, rather than being demolished. This is a relevant question when sustainability, key in the paradigm of the circular economy, is considered. Most structural steel design codes do not provide specific guidance on post-fire material properties – except BS 5950–8 [25], which is now withdrawn – so the final decision depends on forensic observations, often based on qualitative judgements rather than quantitative findings [26–28]. In fact, a commonly accepted indicator for reinstating a structure is that the permanent deformations experienced by the load-bearing elements are not excessively high.

In the current paper, an experimental study to assess the post-fire performance of HSS, accounting for a combination of high temperature and tensile loading, is presented. S700 test specimens were cut from hot-rolled plates and extracted from cold-formed circular hollow sections (CHS). Transient-state tests were conducted to obtain the *critical temperature* θ_{crit} causing failure under a combination of tensile load and steadily increasing temperature. Subsequently, post-fire tests were

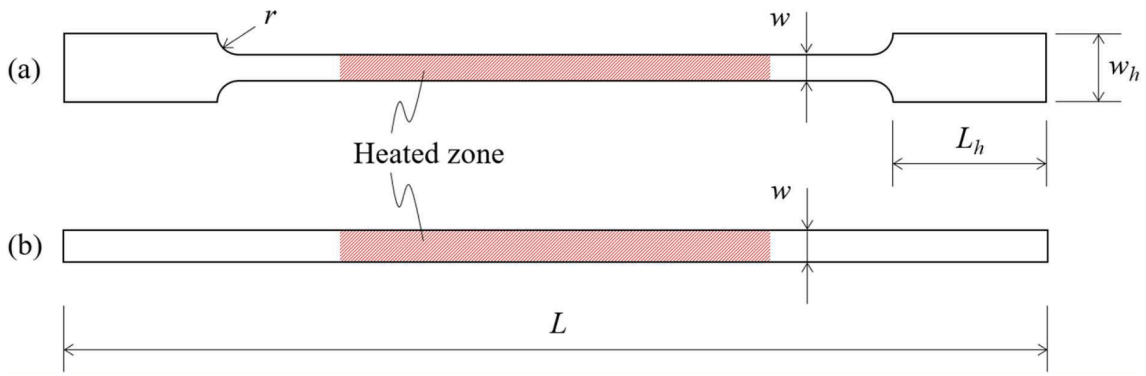


Fig. 2. Test specimens (units in mm). (a) Dogbone coupons for Sets 1–2. (b) Prismatic coupons for Sets 3–6.

Table 2
Details and nominal geometrical properties of test coupons.

Steel grade	Set	Product	Production route	w (mm)	t (mm)	w_h (mm)	L_h (mm)	r_h (mm)	L (mm)
S700	1	Plate	HR	20	8	60	150	20	800
	2	Plate	HR	15	12	60	150	20	
	3	CHS-A	TR+CF	27	4	–	–	–	
	4	CHS-B	TR+CF	18	5	–	–	–	
	5	CHS-C	TR+CF	18	6	–	–	–	
S355	6	S355 CHS	CF	23	6	–	–	–	800

HR: hot-rolled. TR: thermomechanically rolled. CF: cold-formed.

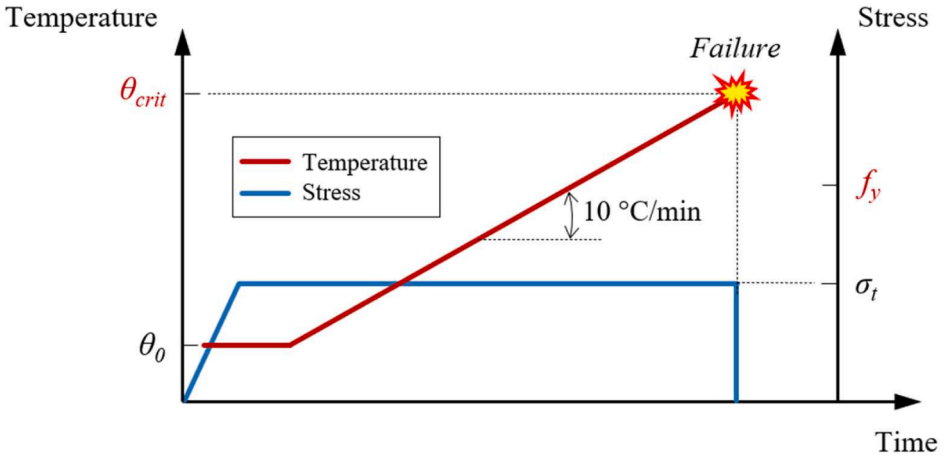


Fig. 3. Temperature and stress histories in transient-state tests.

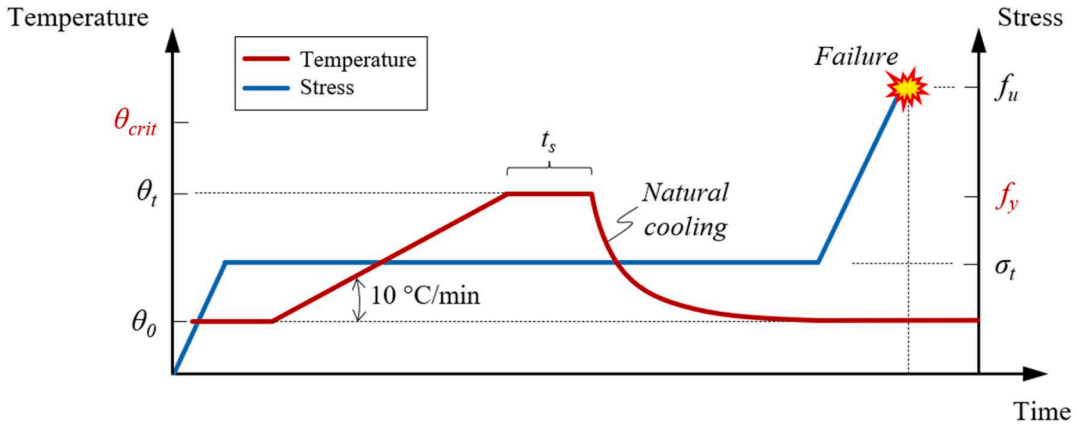


Fig. 4. Temperature and stress histories in post-fire tests.

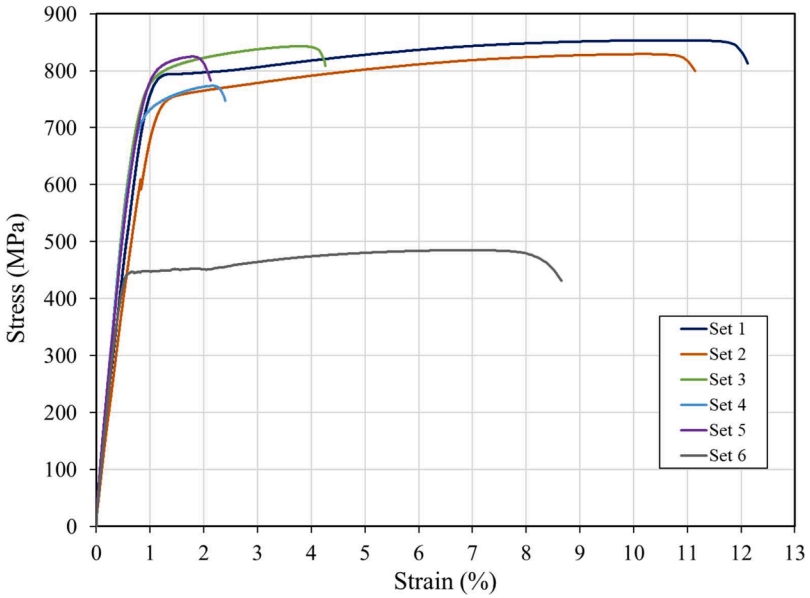


Fig. 5. Average stress-strain curves at room temperature for the six specimen sets.

Table 3
Average mechanical properties of specimens at room temperature.

Steel grade	Set	f_y (MPa)	f_u (MPa)	ε_u (%)	ε_f (%)	E (MPa)
S700	1	777.3	853.5	10.46	13.00	205,000
	2	721.5	829.1	10.20	12.36	201,000
	3	754.8	842.9	3.74	4.74	209,000
	4	714.1	773.6	2.15	2.90	220,000
	5	769.3	824.8	1.76	2.77	221,000
S355	6	446.8	484.9	6.73	9.21	208,000

conducted on both unloaded and loaded specimens that were heated to a target temperature $\theta_t < \theta_{crit}$ and cooled in air prior to being submitted to tensile testing. By means of these tests, the residual mechanical properties (yield strength, ultimate strength, Young's modulus, ultimate strain and strain at fracture) were examined, with a special focus on the residual ductility of the material. The results were compared with existing data on S355 steel and with the ductility requirements set out in Eurocode 3.

2. Materials and methods

2.1. Experimental setup

The experimental setup, which was utilized by the authors in previous investigations to perform tensile tests at room and high temperatures [38] is depicted in Fig. 1. The setup includes a hydraulic universal testing machine equipped with a 200 kN calibrated load cell. The upper and lower blocks of the machine housed flat hydraulic jaws, by means of which each specimen was laterally clamped at both ends to prevent slipping. During the tensile tests, the upper block remained stationary while the lower moved downward.

The specimens were heated to temperatures up to 1000 °C using an electric furnace that featured three independently controlled heating zones located in the upper, middle and lower third of the heating chamber. K-type thermocouples were employed to regulate the temperature of each heating zone, which served as feedback variables for precise control of the heating. The upper and lower furnace openings were sealed with rock wool, ensuring evenly distributed temperature within the heating chamber. An extensometer with a gauge length of 50 mm was positioned in the central section of each specimen.

The data obtained from the extensometer, the machine displacements, as well as the thermocouple readings, were digitally recorded at a sampling frequency of 2 Hz using dedicated software. The data were used to plot the stress-strain curves, as well as to compute the key mechanical properties, including the yield strength, ultimate strength, ultimate strain, strain at fracture and Young's modulus.

2.2. Test specimens

Five sets of S700 steel specimens were tested, covering two production routes and two section types: hot-rolled plates and cold-formed circular hollow sections (CHS) produced from thermomechanically rolled plate. One additional set of S355 steel specimens was also considered to compare the post-fire behaviour of high-strength steels with normal strength steels. Table 1 shows the chemical composition of the steels.

Sets 1 and 2 consisted of dogbone coupons that were laser-cut from S700 MC hot-rolled steel plates of 8 mm and 12 mm-thickness, respectively. Sets 3–5 consisted of curved prismatic coupons cut longitudinally (away from the weld seam) from 3 different cold-formed S700 steel circular hollow sections (CHS), designated as CHS-A, CHS-B and CHS-C. Set 6 consisted of coupons that were cut from a batch of CHS that were cold-formed from 6 mm-thick S355 steel plate. Fig. 2 depicts the geometry of the coupons, and their thicknesses t and widths w are listed in Table 2. All the specimens had a total length of 800 mm to exceed the furnace height and be properly clamped in the testing machine (see Fig. 1). The total heated length, i.e., the length of the heating chamber, was 350 mm.

2.3. Test procedures

In the present work, three test procedures were used.

2.3.1. Room temperature tests

To measure the key mechanical properties of each set of specimens at room temperature, three specimens of each set underwent tensile testing. The stress-strain curves were derived from these tests, and the mechanical properties were extracted, including yield strength, ultimate strength, ultimate strain, strain at fracture and Young's modulus.

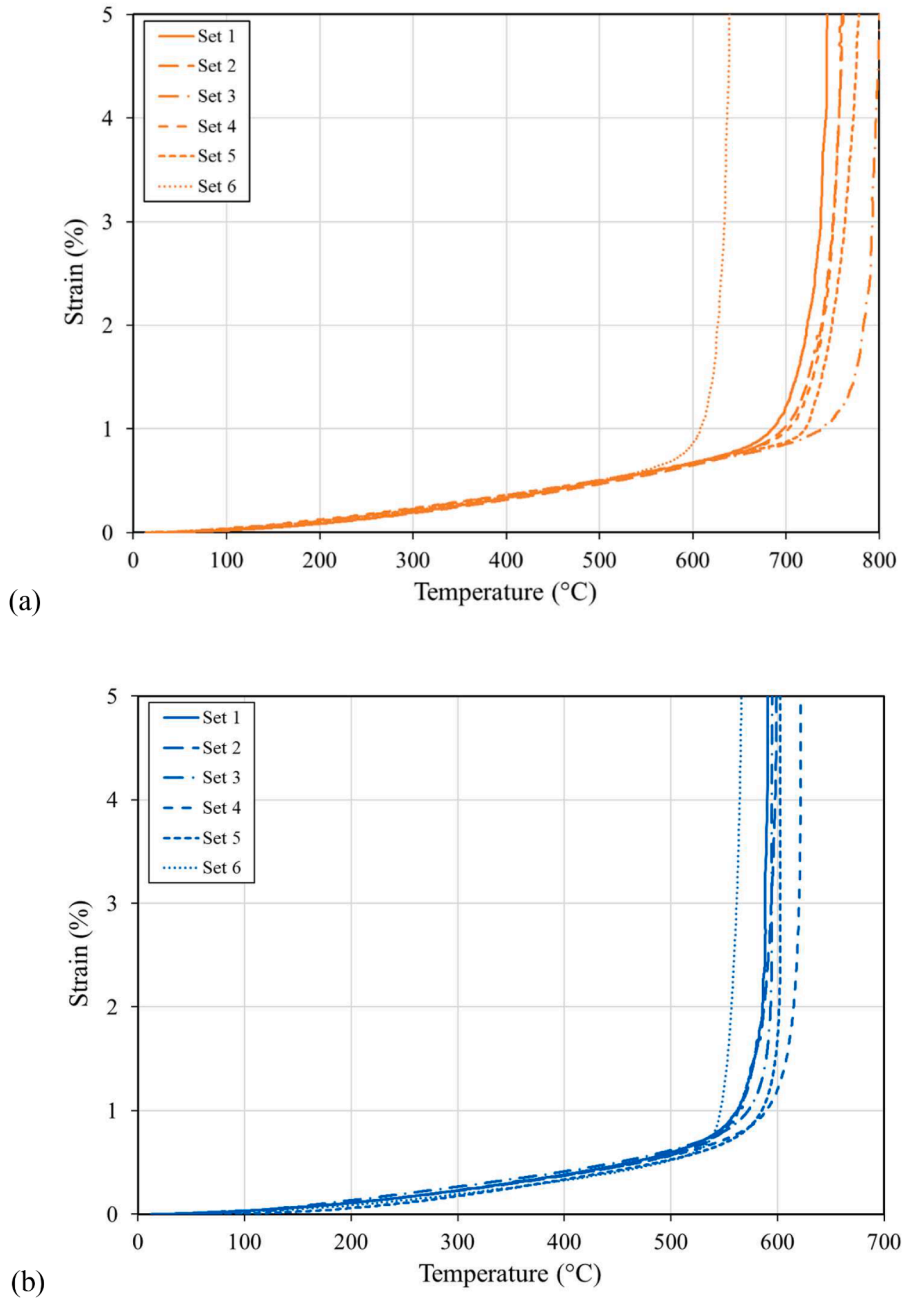


Fig. 6. Strain-temperature histories recorded from transient-state tests for specimens subjected to three degrees of utilisation: (a) $\mu_0 = 0.2$, (b) $\mu_0 = 0.5$ and (c) $\mu_0 = 0.7$.

2.3.2. *Transient-state tests*

Transient-state tests are designed to replicate the combined effects of uniform load and increasing temperature acting on a structural material during a fire. This approach provides a more realistic representation and comprehensive understanding of the material behaviour under fire conditions compared to traditional steady-state tests, in which the specimen undergoes tensile testing once a target temperature is reached (see, for example, [13] and [40]).

The experimental procedure used to perform the transient-state tests is illustrated in the temperature and stress histories of Fig. 3.

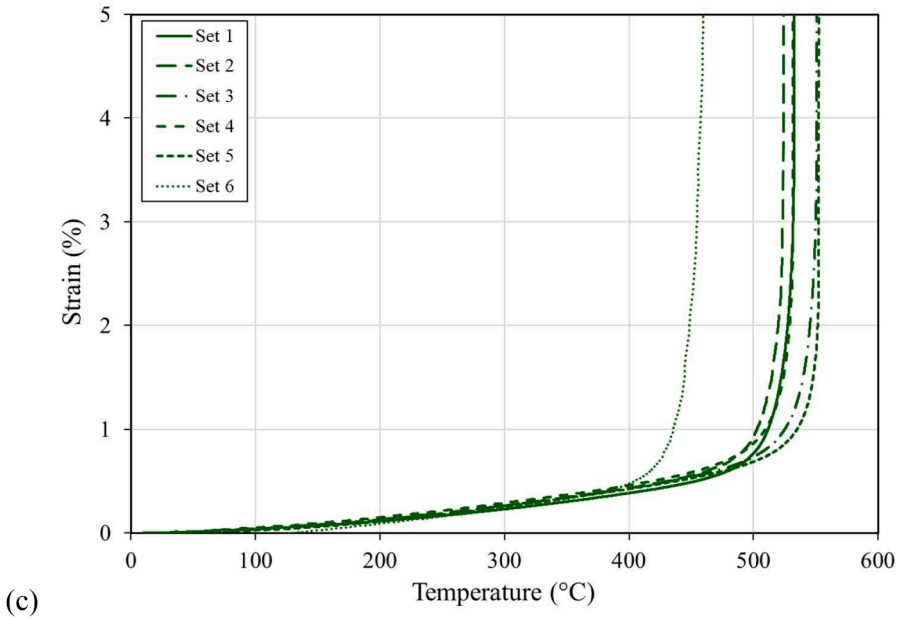
The coupon specimens were placed in the testing machine, clamped at both ends and subjected to a tensile load that induced a target tensile stress σ_t corresponding to a specified proportion of the measured yield strength f_y of the material at room temperature. The target stress σ_t was determined by means of the following expression:

$$\sigma_t = \mu_0 f_y \tag{1}$$

where $\mu_0 \in (0,1)$ is a parameter known as the *degree of utilisation* in EN 1993–1-2 [41], which represents the stress level a steel member bears during a fire. This parameter can be used to approximate the load level in a real fire scenario (assuming a strength, rather than stability dominated failure mode). Thus:

$$\mu_0 = \frac{E_{fi,d}}{R_{fi,d,0}} \tag{2}$$

where $E_{fi,d}$ is the design effect of an action in the fire situation and $R_{fi,d,0}$ is the design value of the member resistance in the fire situation at the



(c)

Fig. 6. (*continued*).

Table 4
Critical temperatures θ_{crit} (μ_0) (°C) measured from the specimens of each test set.

Degree of utilisation μ_0	Critical temperature θ_{crit} (°C)					
	Set 1	Set 2	Set 3	Set 4	Set 5	Set 6
0.1	882	885	879	868	907	811
0.2	747	767	762	757	782	646
0.3	676	706	693	692	709	602
0.4	641	654	644	646	657	560
0.5	591	600	607	611	617	553
0.6	560	542	576	582	584	495
0.7	533	524	550	557	556	448
0.8	463	459	527	536	532	440
0.9	423	451	507	517	511	422

onset of the fire. In this work, as given by Eq. (1), the degree of utilisation μ_0 of every tested specimen was computed as the ratio of the applied tensile stress σ_t to the yield strength f_y at room temperature. According to Fig. 3, the target stress σ_t was applied and held constant for the entire duration of each test, while the specimen was subjected to a heating rate of 10 °C/min. This value is approximately the heating rate of partially protected steel elements during a natural fire, and it was chosen to allow comparisons with similar studies that used the same heating rate [42,43].

Each transient-state test was concluded upon the first occurrence of either failure of the specimen or attainment of the maximum stroke of the testing machine. The temperature at the end of the test, for a given degree of utilisation μ_0, was recorded and referred to as the *critical temperature* θ_{crit} (μ_0). For each specimen set and degree of utilisation μ_0, the critical temperature was computed as the average of two tests.

2.3.3. Post-fire tests

Post-fire tests are performed to obtain the residual mechanical properties of steel specimens after being heated to high temperatures and subsequently cooled down to room temperature. The test methodology is illustrated in the time-dependant histories of Fig. 4. The specimens were placed in the testing machine, clamped at both ends and subjected to a preload at room temperature θ_0 up to a tensile stress level σ_t (μ_0) computed according to Eq. (1). The same degrees of utilisation μ_0 employed for the transient-state tests were also considered for the post-fire tests. Subsequently, the specimens underwent controlled heating at a constant heating rate of 10 °C/min, which concluded when a target temperature $\theta_t < \theta_{crit}$ (μ_0) was reached. Thus, unlike in the transient-state tests, the specimens did not fail. The heating rate was kept consistent with the transient-state tests to avoid introducing additional variables into the experiments.

Upon achieving the target temperature, the temperature was held for a soaking time $t_s = 30$ min to ensure uniform heating throughout the specimen. Once the specimens had been evenly heated, the furnace was turned off and gradually opened, allowing the specimen to cool down naturally in air to room temperature θ_0. Finally, the tensile stress σ_t (μ_0) (that had thus far been kept constant) was increased until the failure of the specimen was reached at its ultimate strength f_u. Following this procedure, the combined influence of load and temperature on the post-fire behaviour of HSS can be considered in a realistic manner, reflecting the fact that steel structures carry a certain amount of load during fires.

To study the combined influence of the target temperature θ_t and the degree of utilisation μ_0 on the residual properties of the specimens after fire, two types of post-fire tests were performed. In the first type of test, referred to hereinafter as post-fire, unloaded tests (PFU, see sub-Section 3.3.1, the specimens were heated to the target temperature θ_t without bearing tensile stress (i.e., $\mu_0 = 0$). Since there was no load acting on the specimens, the specimens were allowed to deform freely. In the second type of test, referred to hereinafter as post-fire, loaded tests (PFL, see sub-Section 3.3.2), the specimens were subjected to a combination of tensile stress σ_t (μ_0), with $\mu_0 > 0$, and heating to the target temperature $\theta_t < \theta_{crit}$ (μ_0).

While PFU tests are frequently used to obtain the residual properties of structural steels due to their practicality and ease of implementation, PFL tests provide a close representation of a real fire scenario. In the post-fire tests, for each specimen set and target temperature, two specimens were tested.

3. Results

3.1. Material properties at room temperature

The stress-strain curves derived from the tensile tests at room temperature are depicted in Fig. 5. From these curves, the key mechanical properties of the material were extracted, and the average values are presented in Table 3, including the yield strength (taken as the 0.2 %

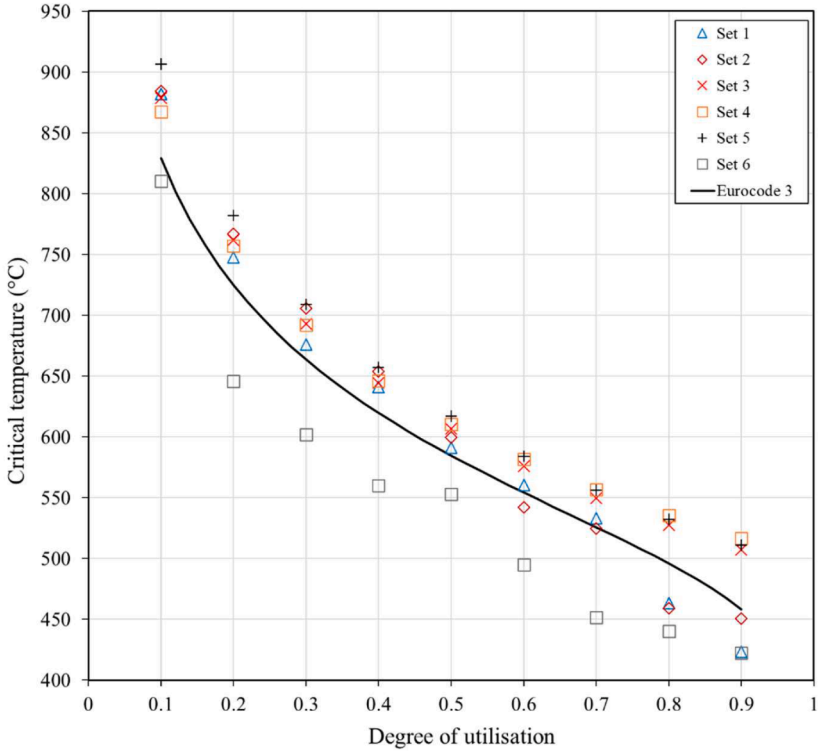


Fig. 7. Variation of critical temperature with degree of utilisation for each specimen set from transient-state tests.

proof strength) f_y, the ultimate strength f_u, the Young's modulus E, the ultimate strain ε_u (strain at f_u) and the fracture strain ε_f, measured over 50 mm.

Some variation in Young's modulus and strength was observed between the different S700 samples, but the most pronounced differences were seen in the values of ε_u and ε_f, with the cold-formed sections showing substantially reduced ductility due to the effects of cold-work during forming [44–46].

3.2. Critical temperatures obtained from transient-state tests

Transient-state tests were performed at various degrees of utilisation $\mu_0 \in (0.1 - 0.9)$, in increments of 0.1. The variation in strain with temperature was recorded during each test, as shown in Fig. 6 for the different specimen sets tested in this work for three degrees of utilisation: low ($\mu_0 = 0.2$), medium ($\mu_0 = 0.5$) and high ($\mu_0 = 0.7$). All the $\varepsilon - \theta$ curves in Fig. 6 began at zero strain because the initial strain caused by the tensile stress that was applied at the beginning of each test was excluded. As expected, the strain rate rose with temperature for a given degree of utilisation μ_0. For the tests in which the specimen failed, the critical temperature θ_{crit} (μ_0) was taken as the 'runaway value' because when this value was attained, the strain rate $d\varepsilon/dt$ reached a maximum in the heating history, and subsequently the strains rose sharply.

The measured critical temperatures are presented in Table 4. As expected, the higher the tensile stress σ_t (μ_0) to which the specimen was subjected, the lower the value of θ_{crit} (μ_0). The critical temperature test results are plotted against the degree of utilisation in Fig. 7, where some variation between the results obtained from the different specimen sets may be observed. For comparison purposes, the EN 1993–1-2 [41] $\theta_{crit} - \mu_0$ relationship for normal strength steel, as given by Eq. (3), is also shown.

$$\theta_{crit}(\mu_0) = 39.16 \ln\left(\frac{1}{0.9674\ {\mu_0}^{3.833}} - 1\right) + 482 \tag{3}$$

As with the Eurocode 3 curve, the experimental values of θ_{crit} (μ_0) for each specimen set show a decreasing logarithmic trend (the fitting curves are not presented for reasons of clarity but have a coefficient of determination $R^2 > 0.97$). A similar trend was found in previous work by the authors regarding the influence of the load level on the critical temperature of steel reinforcing bars [38]. It can be seen that the production route has a notable influence on the critical temperature of the S700 steel specimens at the higher degrees of utilisation.

3.3. Residual mechanical properties from post-fire test results

3.3.1. Post-fire, unloaded tests (PFU)

In order to assess the influence of steel grade and production route on the post-fire behaviour of structural steel, the residual stress-strain curves obtained from the PFU tests are compared in Fig. 8a for the S700 hot-rolled 8-mm thick steel plate material (Set 1), Fig. 8b for the corresponding 12-mm thick material (Set 2) and Fig. 8c for the S355 steel specimens extracted from the CHS (Set 6). The specimens were heated to target temperatures θ_t ranging from 300 °C to 1000 °C (at intervals of 100 °C) and subsequently cooled back down to room temperature θ_0. As observed in previous studies [32,37,47], heating to temperatures below 200 °C has a negligible influence on the post-fire behaviour of the material. The stress-strain curve obtained from the room temperature tests is also plotted in each graph for comparison purposes. Only a limited number of specimens could be extracted from the S700 steel CHS; hence, PFL tests were prioritized for these sets, and just a few PFU tests were carried out, the results of which are presented with the PFL test results. The key residual mechanical properties (yield strength f_y, ultimate strength f_u, Young's modulus E, ultimate strain ε_u and strain at fracture ε_f) were extracted from the stress-strain curves and are presented in Tables 5–7, together with the 'residual factors', i.e., the ratios between the residual value of a mechanical property measured after a PFU test to the value of that property measured at room temperature (Table 3).

For the S700 steel specimens cut from hot-rolled plates, i.e., Sets 1 and 2, the yield strength, ultimate strength and Young's modulus were essentially unaffected after the material had been heated to peak temperatures up to 600 °C, while the ductility showed some variation. When

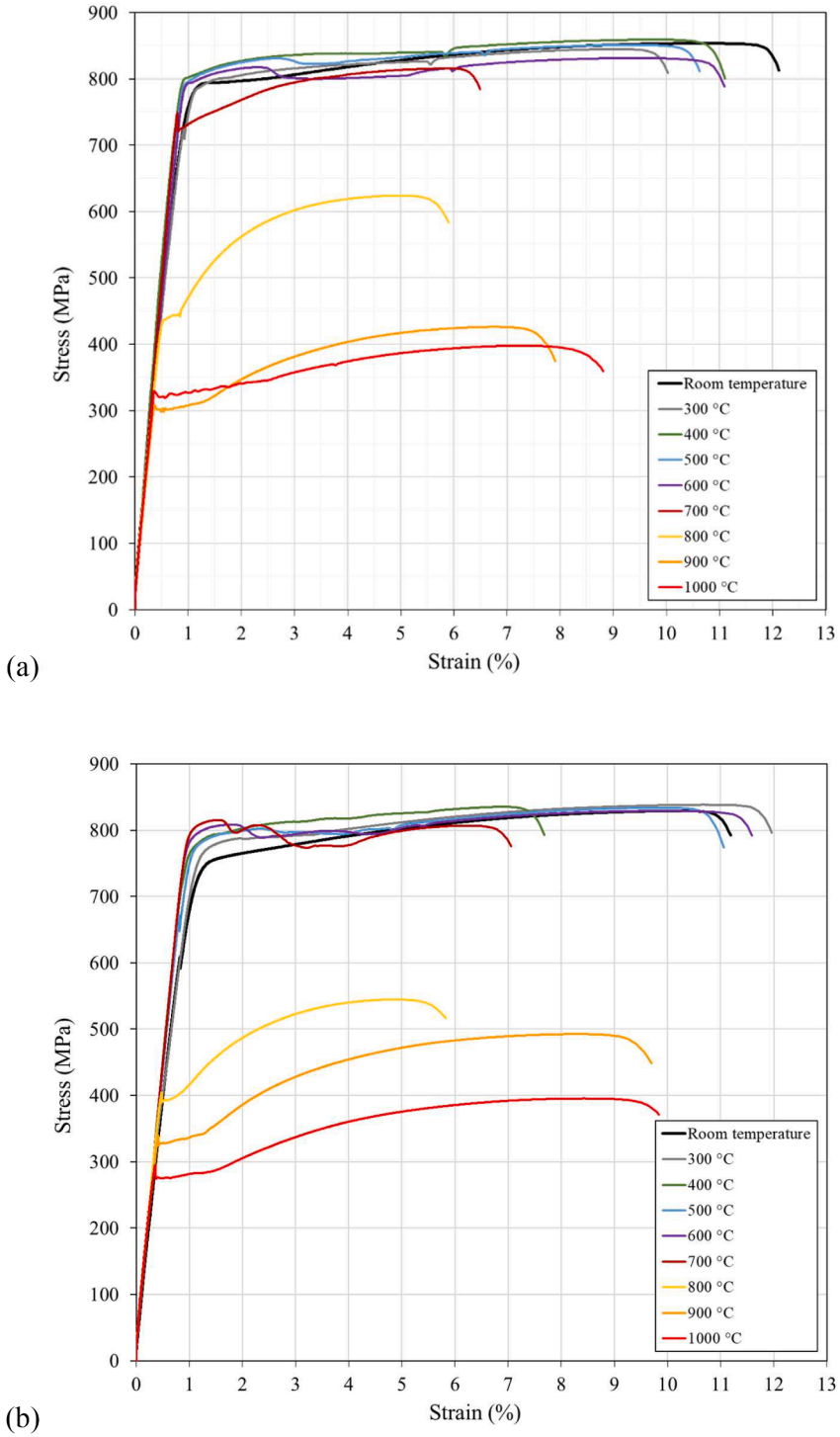
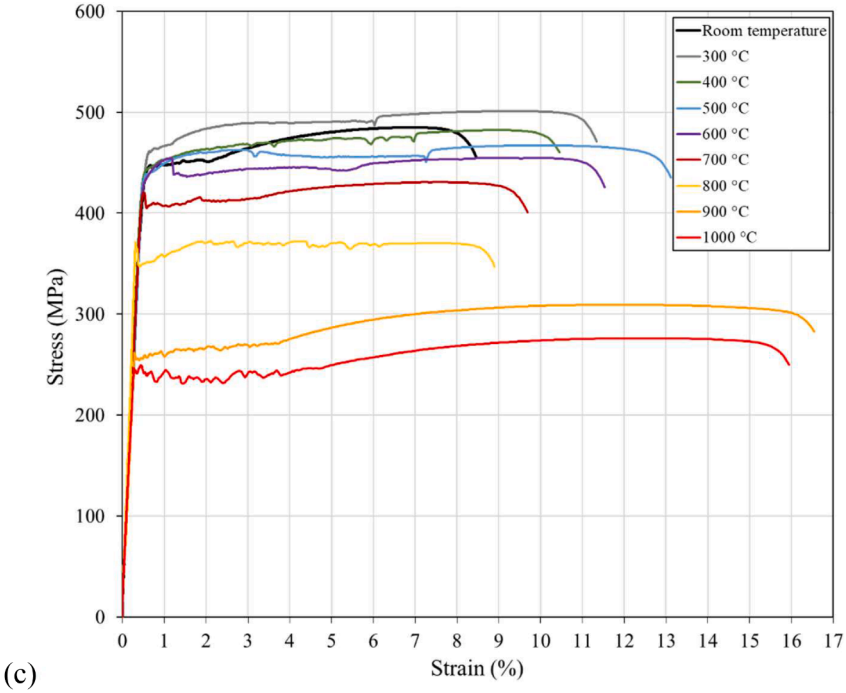


Fig. 8. Residual stress-strain curves obtained from PFU tests: (a) S700 steel specimens cut from hot-rolled 8 mm plates (Set 1), (b) S700 steel specimens cut from hot-rolled 12 mm plates (Set 2) and (c) S355 specimens cut from CHS.

heated to 700 °C or above, material deterioration is evident in both plate thicknesses. For both specimen thicknesses, a substantial reduction of ductility is observed following exposure to temperatures up to 800 °C, but the trend reverses for 900 °C and 1000 °C. This has been seen in previous studies [38] and related to the phase changes that occur in HSS within the range of 700 °C – 800 °C.

For the specimens extracted from the S355 CHS (see Fig. 8c and Table 7) it can be seen that heating up to 400 °C leads to an increase in the residual values of the mechanical properties with respect to those measured at room temperature. Within the range 500 °C – 700 °C, the residual values of the yield and tensile strength reduce slightly, but their properties are mostly retained (about 90 % when heated up to 700 °C). However, following exposure to 800 °C or higher temperatures, the residual properties reduce drastically. By 1000 °C, the residual factors for both yield and tensile strengths reduce to less than 0.6. As can be seen in the stress-strain curves of Fig. 8, residual ductility slightly increases for the entire range of target temperatures. It is noteworthy to observe that the residual ductility almost doubles after heating to 900 °C and 1000



(c)

Fig. 8. (*continued*).

Table 5
Residual values and factors for key mechanical properties obtained from PFU tests on S700 steel specimens cut from 8 mm hot-rolled plates (Set 1).

θ_t (°C)	Yield strength		Ultimate strength		Ultimate strain		Strain at fracture		Young's modulus	
	$f_{y,\theta}$ (MPa)	$f_{y,\theta}/f_y$	$f_{u,\theta}$ (MPa)	$f_{u,\theta}/f_u$	$\varepsilon_{u,\theta}$ (%)	$\varepsilon_{u,\theta}/\varepsilon_u$	$\varepsilon_{f,\theta}$ (%)	$\varepsilon_{f,\theta}/\varepsilon_f$	E_θ (MPa)	E_θ/E
300	776.1	1.00	844.8	0.99	8.94	0.85	10.84	0.83	210,000	1.02
400	801.3	1.03	859.1	1.01	9.63	0.92	12.03	0.93	217,000	1.06
500	798.3	1.03	850.9	1.00	9.24	0.88	11.50	0.88	210,000	1.02
600	795.0	1.02	831.3	0.97	9.25	0.88	11.89	0.33	192,000	0.94
700	728.1	0.94	815.8	0.96	5.86	0.56	7.33	0.56	198,000	0.97
800	442.7	0.57	623.9	0.73	4.93	0.47	6.70	0.52	200,000	0.98
900	300.3	0.39	426.1	0.50	6.70	0.64	8.48	0.65	227,000	1.11
1000	320.6	0.41	397.8	0.47	7.20	0.69	9.57	0.74	N/A	N/A

N/A: data not available due to measurement errors.

Table 6
Residual values and factors for key mechanical properties obtained from PFU tests on S700 steel specimens cut from 12 mm hot-rolled plates (Set 2).

θ_t (°C)	Yield strength		Ultimate strength		Ultimate strain		Strain at fracture		Young's modulus	
	$f_{y,\theta}$ (MPa)	$f_{y,\theta}/f_y$	$f_{u,\theta}$ (MPa)	$f_{u,\theta}/f_u$	$\varepsilon_{u,\theta}$ (%)	$\varepsilon_{u,\theta}/\varepsilon_u$	$\varepsilon_{f,\theta}$ (%)	$\varepsilon_{f,\theta}/\varepsilon_f$	E_θ (MPa)	E_θ/E
300	764.3	1.06	838.3	1.01	10.64	1.04	13.07	1.06	224,000	1.11
400	771.8	1.07	835.2	1.01	6.90	0.68	8.84	0.72	217,000	1.06
500	771.0	1.07	833.8	1.01	9.68	0.95	12.11	0.98	204,000	1.00
600	791.9	1.10	829.2	1.00	9.78	0.96	12.80	1.04	208,000	1.01
700	805.1	1.12	815.2	0.98	6.15	0.15	8.28	0.67	208,000	1.01
800	393.8	0.55	544.6	0.66	4.82	0.47	6.89	0.56	202,000	0.99
900	328.1	0.45	492.4	0.59	8.15	0.80	10.67	0.86	188,000	0.92
1000	274.8	0.38	395.4	0.48	8.41	0.82	10.95	0.89	N/A	N/A

N/A: data not available due to measurement errors.

°C, with retention factors for ultimate strain and strain at fracture close to 2. As in the S700 steel, the Young's modulus was also unaffected after cooling. In some of the stress-strain curves, stress fluctuations with increasing strains, caused by data sampling errors, are visible.

3.3.2. *Post-fire, loaded tests (PFL)*

In the PFL tests conducted in the present study, the degree of utilisation range $\mu_0 \in (0.1, 0.8)$ was considered. The PFL test campaign is summarized in Table 8 and 9 for Sets 1 and 2, respectively, Table 10 for Sets 3–5 and Table 11 for Set 6. In Tables 8–11, the first two rows show

Table 7
Residual values and factors for key mechanical properties obtained from PFU tests on S355 steel specimens cut from CHS (Set 6).

θ_t (°C)	Yield strength		Ultimate strength		Ultimate strain		Strain at fracture		Young's modulus	
	$f_{y,\theta}$ (MPa)	$f_{y,\theta}/f_y$	$f_{u,\theta}$ (MPa)	$f_{u,\theta}/f_u$	$\varepsilon_{u,\theta}$ (%)	$\varepsilon_{u,\theta}/\varepsilon_u$	$\varepsilon_{f,\theta}$ (%)	$\varepsilon_{f,\theta}/\varepsilon_f$	E_θ (MPa)	E_θ/E
300	459.8	1.03	500.9	1.03	8.99	1.34	12.10	1.31	200,000	0.96
400	445.4	1.00	482.1	0.99	8.83	1.31	11.26	1.22	207,000	0.99
500	441.0	0.99	467.0	0.96	9.65	1.43	13.96	1.52	207,000	0.99
600	441.1	0.99	454.8	0.94	9.70	1.44	12.32	1.34	203,000	0.97
700	407.3	0.91	430.6	0.89	7.62	1.13	10.43	1.13	184,000	0.88
800	349.0	0.78	372.3	0.77	7.59	1.13	9.53	1.03	209,000	1.00
900	255.7	0.57	309.3	0.64	12.00	1.78	17.31	1.88	180,000	0.86
1000	246.2	0.55	276.0	0.57	12.34	1.83	15.99	1.74	193,000	0.93

Table 8
Testing temperatures θ_t and their percentage of θ_{crit} (μ_0) for PFL tests on S700 steel specimens cut from 8 mm hot-rolled plates (Set 1). The shaded cells indicate the cases for which PFL tests were performed.

μ_0	0.1	0.2	0.3	0.4	0.5	0.6	0.7	0.8
θ_{crit} (μ_0) (°C)	882	747	676	641	591	561	533	463
θ_t (°C)	% θ_{crit} (μ_0)							
300	34%	40%	44%	47%	51%	53%	56%	65%
400	45%	54%	59%	62%	68%	71%	75%	86%
500	57%	67%	74%	78%	85%	89%	94%	108%
600	68%	80%	89%	94%	102%	107%	113%	130%
700	79%	94%	104%	109%	118%	125%	131%	151%
800	91%	134%	148%	156%	169%	178%	188%	216%

Table 9
Testing temperatures θ_t and their percentage of θ_{crit} (μ_0) for PFL tests on S700 steel specimens cut from 12 mm hot-rolled plates (Set 2). The shaded cells indicate the cases for which PFL tests were performed.

μ_0	0.1	0.2	0.3	0.4	0.5	0.6	0.7	0.8
θ_{crit} (μ_0) (°C)	885	767	706	654	600	542	526	459
θ_t (°C)	% θ_{crit} (μ_0)							
300	34%	39%	42%	46%	50%	55%	57%	65%
400	45%	52%	57%	61%	67%	74%	76%	87%
500	57%	65%	71%	76%	83%	92%	95%	109%
600	68%	78%	85%	92%	100%	111%	114%	131%
700	79%	91%	99%	107%	117%	129%	133%	153%
800	90%	130%	142%	153%	167%	185%	190%	218%

the degree of utilisation μ_0 and the critical temperature θ_{crit} (μ_0) obtained from the transient-state tests (Table 4), respectively. The first column lists the target temperatures $\theta_t \in [300, 1000]$ °C, which were the same that as those used in the PFU tests. Each value in Tables 8–11 is the ratio θ_t / θ_{crit} (μ_0) expressed as a percentage. For example, Table 8 shows that, if a specimen in Set 1 is loaded ($\mu_0 = 0.5$) and heated up to $\theta_t = 400$ °C,

Table 10
Testing temperatures θ_t and their percentage of $\theta_{crit}(\mu_0)$ for PFL tests on S700 steel specimens cut from CHS (Sets 3–5). The shaded cells indicate the cases for which PFL tests were performed.

μ_0	0.2	0.3	0.5	0.7
$\theta_{crit}(\mu_0)$ (°C)	Set 3 762 Set 4 757 Set 5 782	Set 3 693 Set 4 698 Set 5 709	Set 3 607 Set 4 611 Set 5 617	Set 3 550 Set 4 557 Set 5 556
θ_t (°C)	% $\theta_{crit}(\mu_0)$			
300	Set 3 39% Set 4 40% Set 5 38%	Set 3 43% Set 4 43% Set 5 42%	Set 3 49% Set 4 49% Set 5 49%	Set 3 55% Set 4 54% Set 5 54%
400	Set 3 52% Set 4 53% Set 5 51%	Set 3 58% Set 4 57% Set 5 56%	Set 3 66% Set 4 65% Set 5 65%	Set 3 73% Set 4 72% Set 5 72%
500	Set 3 66% Set 4 66% Set 5 64%	Set 3 72% Set 4 72% Set 5 71%	Set 3 82% Set 4 82% Set 5 81%	Set 3 91% Set 4 90% Set 5 90%
600	Set 3 79% Set 4 79% Set 5 77%	Set 3 87% Set 4 86% Set 5 85%	Set 3 99% Set 4 98% Set 5 97%	
700	Set 3 92% Set 4 92% Set 5 90%			

Table 11
Testing temperatures θ_t and their percentage of $\theta_{crit}(\mu_0)$ for PFL tests on S355 steel specimens cut from CHS (Set 6). The shaded cells indicate the cases for which PFL tests were performed.

μ_0	0.1	0.2	0.3	0.4	0.5	0.6	0.7	0.8
$\theta_{crit}(\mu_0)$ (°C)	810	648	602	560	553	495	455	440
θ_t (°C)	% $\theta_{crit}(\mu_0)$							
300	37%	46%	50%	54%	54%	61%	66%	68%
400	49%	62%	66%	71%	72%	81%	88%	91%
500	62%	77%	83%	89%	90%	101%	109%	114%
600	74%	93%	99%	107%	108%	121%	132%	136%
700	86%	108%	116%	125%	126%	141%	154%	159%
800	99%	123%	133%	143%	145%	162%	176%	182%

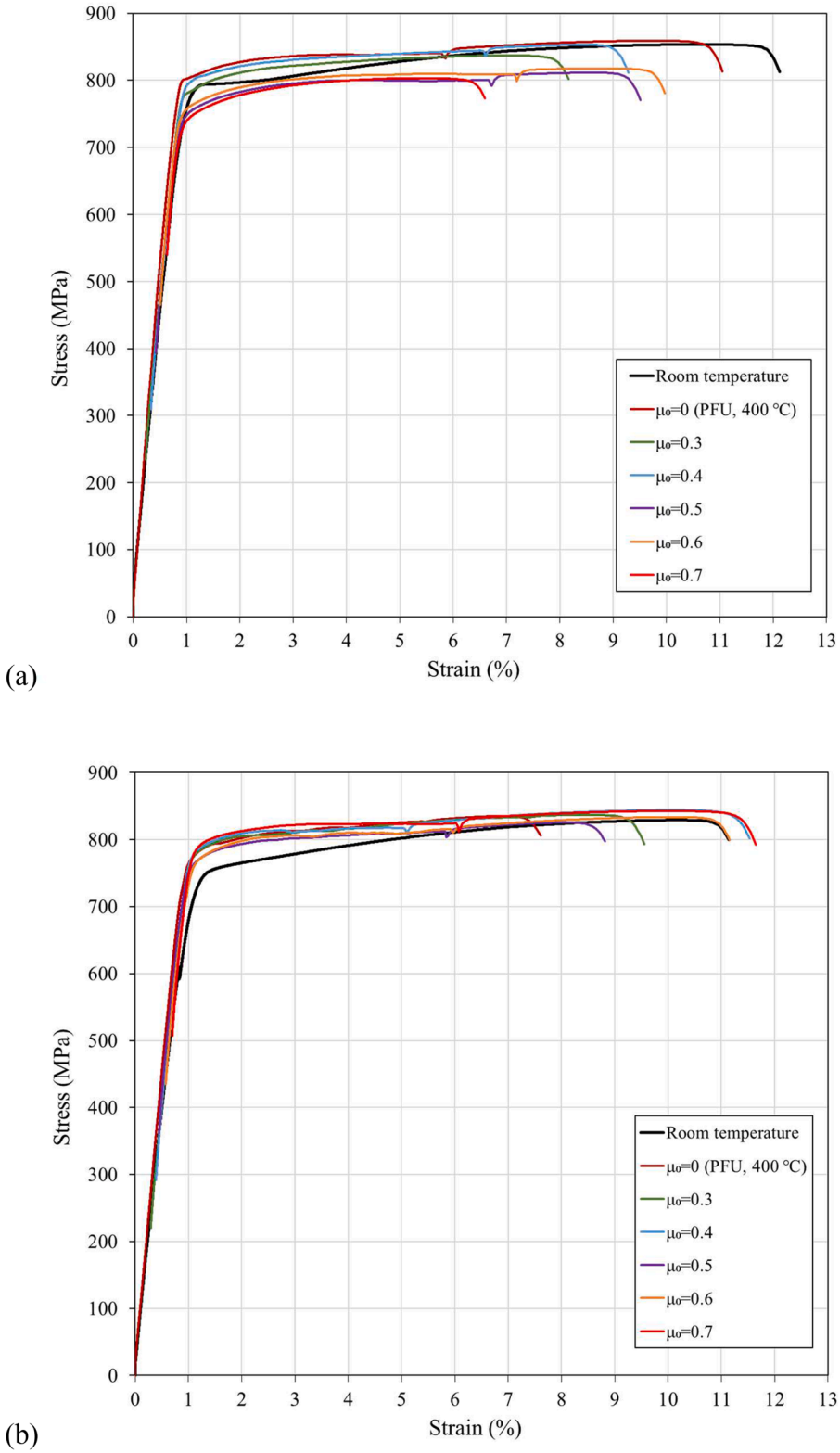
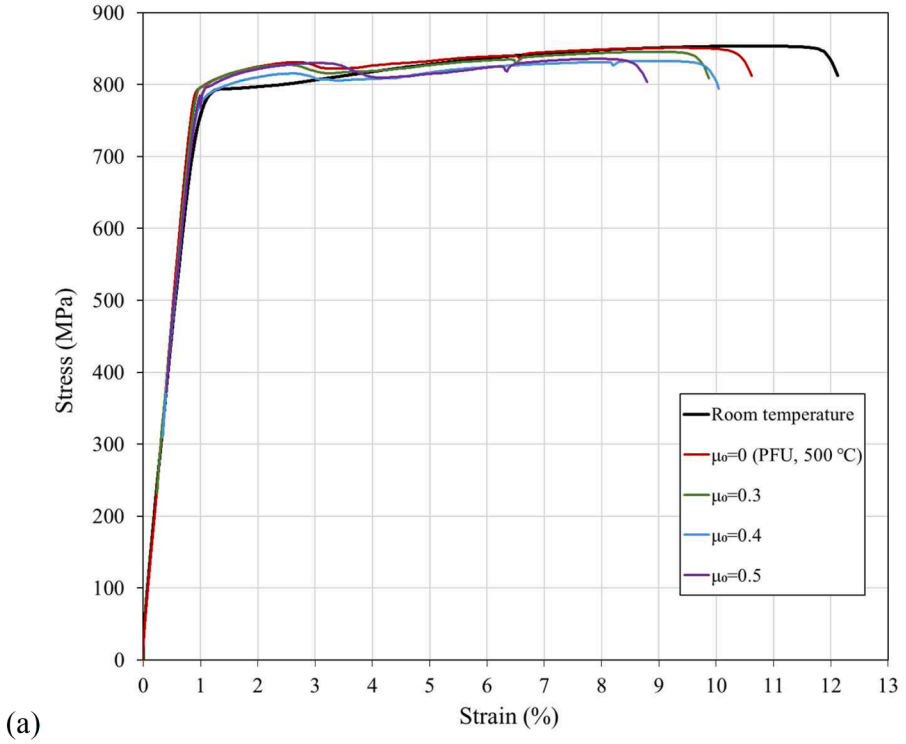


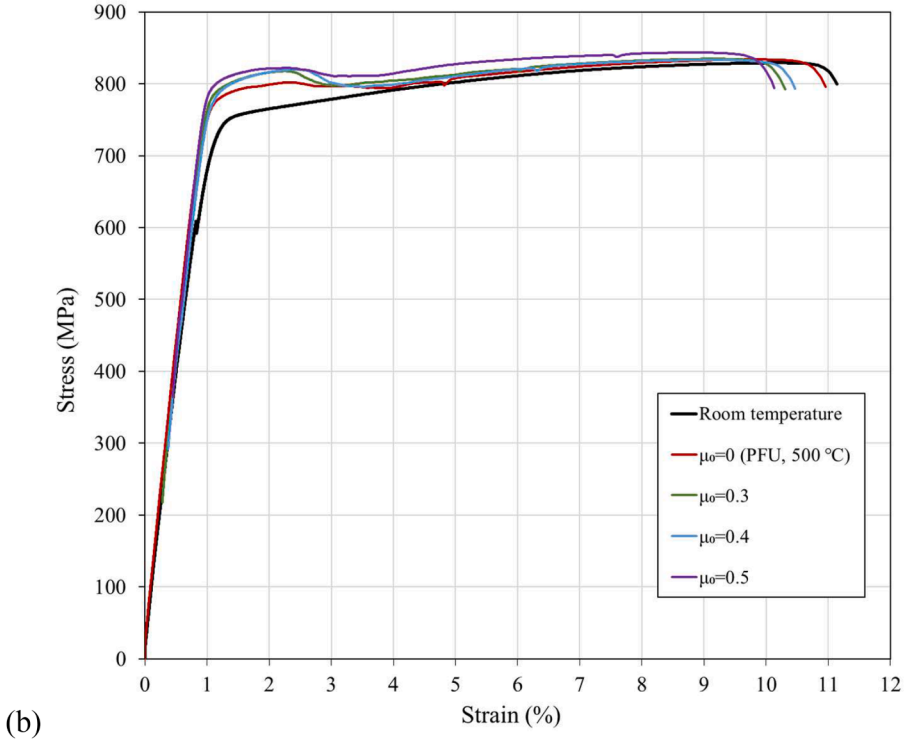
Fig. 9. Residual stress-strain curves obtained from PFL tests performed on S700 steel specimens cut from hot-rolled plates (θ_t = 400 °C and different degrees of utilisation μ_0): (a) t = 8 mm (Set 1) and (b) t = 12 mm (Set 2).

this target temperature is 68 % of the respective critical temperature θ_{crit} (0.5) = 591 °C.

Tests were only performed on a subset (highlighted in blue) of the full matrix, as shown in Tables 8–11, owing to physical limitations (i.e., $\theta_t < \theta_{crit}$ (μ_0)) and practical limitations on the number of test specimens. In the performed tests, the target temperatures were chosen to be mainly within the range 400 °C – 600 °C, corresponding to typical temperatures that structural steel elements may experience during a fire, even if protected. It is interesting to note that, for Sets 1 and 2 (Table 8 and Table 9, respectively), the percentages of the shaded cells for a given testing combination (θ_t, μ_0) differ ± 2 % only, but this difference increases between Sets 1–2 and Set 6 (Table 11).



(a)



(b)

Fig. 10. Residual stress-strain curves obtained from PFL tests performed on S700 steel specimens cut from hot-rolled plates (θ_t = 500 °C and different degrees of utilisation μ_0): (a) t = 8 mm (Set 1) and (b) t = 12 mm (Set 2).

Table 12
Residual values and factors for key mechanical properties obtained from PFL tests ($\theta_t = 400$ °C and different degrees of utilisation μ_0) on S700 steel specimens cut from 8 mm hot-rolled plates (Set 1).

μ_0	Yield strength		Tensile strength		Ultimate strain		Strain at fracture		Young's modulus	
	$f_{y,\theta}$ (MPa)	$f_{y,\theta}/f_y$	$f_{u,\theta}$ (MPa)	$f_{u,\theta}/f_u$	$\varepsilon_{u,\theta}$ (%)	$\varepsilon_{u,\theta}/\varepsilon_u$	$\varepsilon_{f,\theta}$ (%)	$\varepsilon_{f,\theta}/\varepsilon_f$	E_θ (MPa)	E_θ/E
0	801.3	1.03	859.1	1.01	9.63	0.92	12.00	0.92	217,000	1.06
0.3	783.1	1.01	837.0	0.98	7.04	0.67	9.04	0.70	207,000	1.01
0.4	799.5	1.03	853.0	1.00	8.29	0.79	10.07	0.77	210,000	1.02
0.5	751.0	0.97	811.4	0.95	8.56	0.82	10.31	0.79	216,000	1.05
0.6	758.6	0.98	817.7	0.96	8.67	0.83	10.83	0.83	208,000	1.01
0.7	743.0	0.96	803.3	0.94	5.33	0.51	7.44	0.57	198,000	0.97

Table 13
Residual values and factors for key mechanical properties obtained from PFL tests ($\theta_t = 400$ °C and different degrees of utilisation μ_0) on S700 steel specimens cut from 12 mm hot-rolled plates (Set 2).

μ_0	Yield strength		Tensile strength		Ultimate strain		Strain at fracture		Young's modulus	
	$f_{y,\theta}$ (MPa)	$f_{y,\theta}/f_y$	$f_{u,\theta}$ (MPa)	$f_{u,\theta}/f_u$	$\varepsilon_{u,\theta}$ (%)	$\varepsilon_{u,\theta}/\varepsilon_u$	$\varepsilon_{f,\theta}$ (%)	$\varepsilon_{f,\theta}/\varepsilon_f$	E_θ (MPa)	E_θ/E
0	771.8	1.07	835.2	1.01	6.90	0.68	8.84	0.72	217,000	1.08
0.3	781.2	1.08	836.8	1.01	8.35	0.82	10.62	0.86	207,000	1.03
0.4	784.6	1.09	843.9	1.02	10.03	0.98	12.71	1.03	208,000	1.04
0.5	766.3	1.06	825.4	1.00	8.04	0.79	9.97	0.81	222,000	1.11
0.6	765.3	1.06	833.5	1.01	9.90	0.97	12.26	0.99	226,000	1.12
0.7	791.0	1.10	842.5	1.02	9.95	0.98	12.63	1.02	198,000	0.99

Table 14
Residual values and factors for key mechanical properties obtained from PFL tests ($\theta_t = 500$ °C and different degrees of utilisation μ_0) on S700 steel specimens cut from 8 mm hot-rolled plates (Set 1).

μ_0	Yield strength		Tensile strength		Ultimate strain		Strain at fracture		Young's modulus	
	$f_{y,\theta}$ (MPa)	$f_{y,\theta}/f_y$	$f_{u,\theta}$ (MPa)	$f_{u,\theta}/f_u$	$\varepsilon_{u,\theta}$ (%)	$\varepsilon_{u,\theta}/\varepsilon_u$	$\varepsilon_{f,\theta}$ (%)	$\varepsilon_{f,\theta}/\varepsilon_f$	E_θ (MPa)	E_θ/E
0	798.3	1.03	850.9	1.00	9.24	0.88	11.50	0.88	210,000	1.03
0.3	799.6	1.03	845.6	0.99	8.88	0.85	10.73	0.83	215,000	1.05
0.4	782.9	1.01	832.9	0.98	8.66	0.83	10.96	0.84	214,000	1.04
0.5	797.0	1.03	835.7	0.98	7.89	0.75	9.72	0.75	203,000	0.99

Table 15
Residual values and factors for key mechanical properties obtained from PFL tests ($\theta_t = 500$ °C and different degrees of utilisation μ_0) on S700 steel specimens cut from 12 mm hot-rolled plates (Set 2).

μ_0	Yield strength		Tensile strength		Ultimate strain		Strain at fracture		Young's modulus	
	$f_{y,\theta}$ (MPa)	$f_{y,\theta}/f_y$	$f_{u,\theta}$ (MPa)	$f_{u,\theta}/f_u$	$\varepsilon_{u,\theta}$ (%)	$\varepsilon_{u,\theta}/\varepsilon_u$	$\varepsilon_{f,\theta}$ (%)	$\varepsilon_{f,\theta}/\varepsilon_f$	E_θ (MPa)	E_θ/E
0	771.0	1.07	833.8	1.01	9.68	0.95	12.11	0.98	204,000	1.01
0.3	791.0	1.10	834.7	1.01	9.10	0.89	11.59	0.94	201,000	1.00
0.4	788.4	1.09	833.4	1.01	9.07	0.89	11.71	0.95	199,000	0.99
0.5	801.5	1.11	843.4	1.02	8.81	0.86	11.21	0.91	204,000	1.02

From each PFL test carried out, the residual stress-strain curves for the S700 steel specimens cut from plates for two target temperatures and different degrees of utilisation ($\theta_t = 400$ °C, μ_0) and ($\theta_t = 500$ °C, μ_0) are depicted for Sets 1 and 2 in Figs. 9 and 10, respectively. The room temperature stress-strain curves, as well as the residual stress-strain curves obtained from PFU tests at the same target temperatures θ_t, are also plotted for reference purposes. From the residual stress-strain curves, the residual values and factors of the key mechanical properties were extracted, as provided in Table 12-15.

For the S700 steel CHS (Sets 3–5), a limited number of coupons could be extracted due to physical constraints. According to this, specimens from Set 3 and Set 4 were subjected to a target temperature $\theta_t = 500$ °C and different degrees of utilisation μ_0 (Fig. 11). On the other hand, the specimens from Set 5 were subjected to target temperatures ranging from 400 °C to 600 °C with different degrees of utilisation μ_0 (Fig. 12). In Figs. 11 and 12 and 12, the stress-strain curves obtained from the tensile tests at room temperature and the stress-strain curves from the PFU tests at the same target temperatures θ_t are also shown when available. Table 16 summarizes the residual values and factors extracted from the stress-strain curves.

In order to compare the results of PFL tests performed on different products, additional PFL tests were carried out on specimens extracted

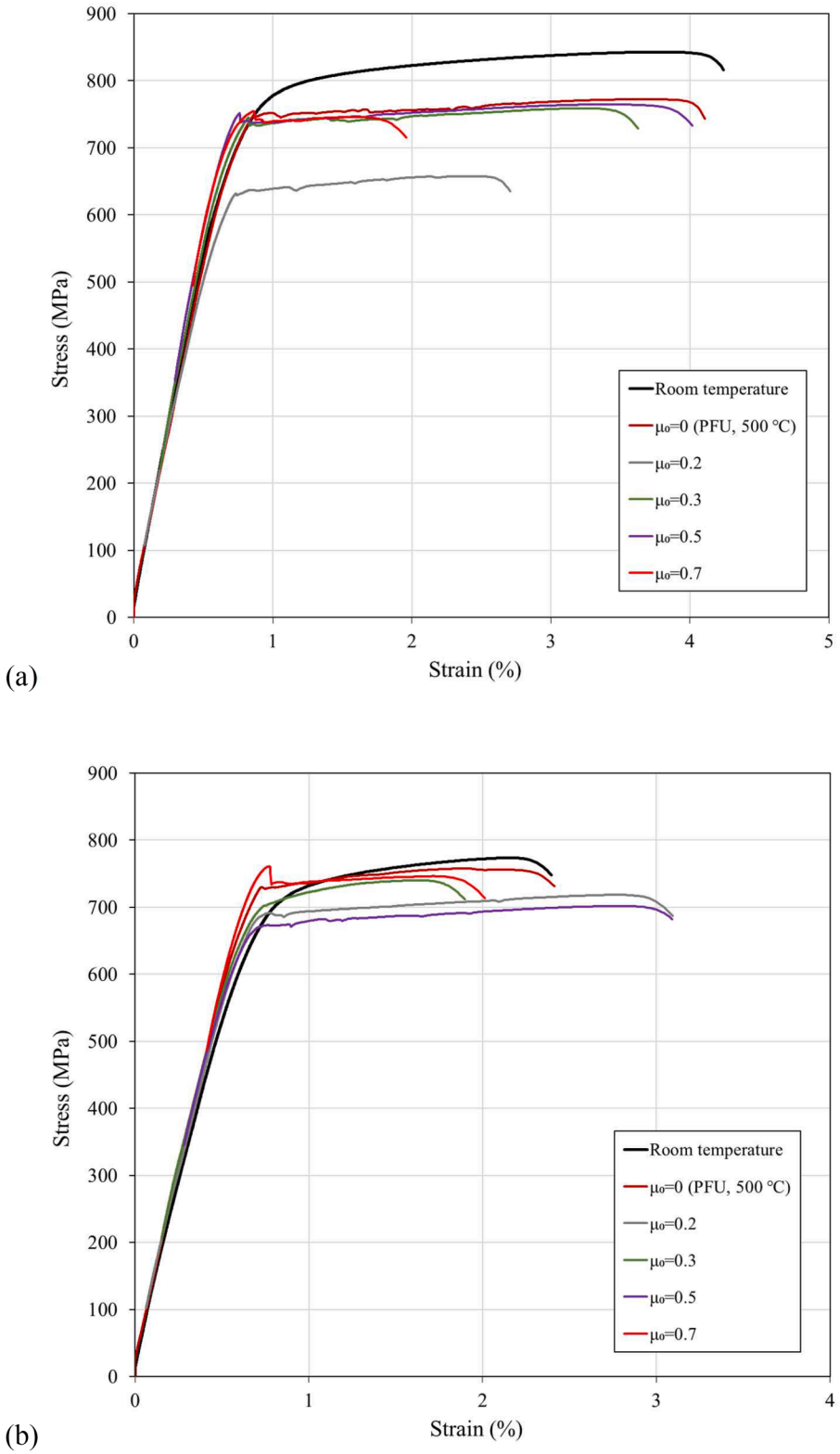
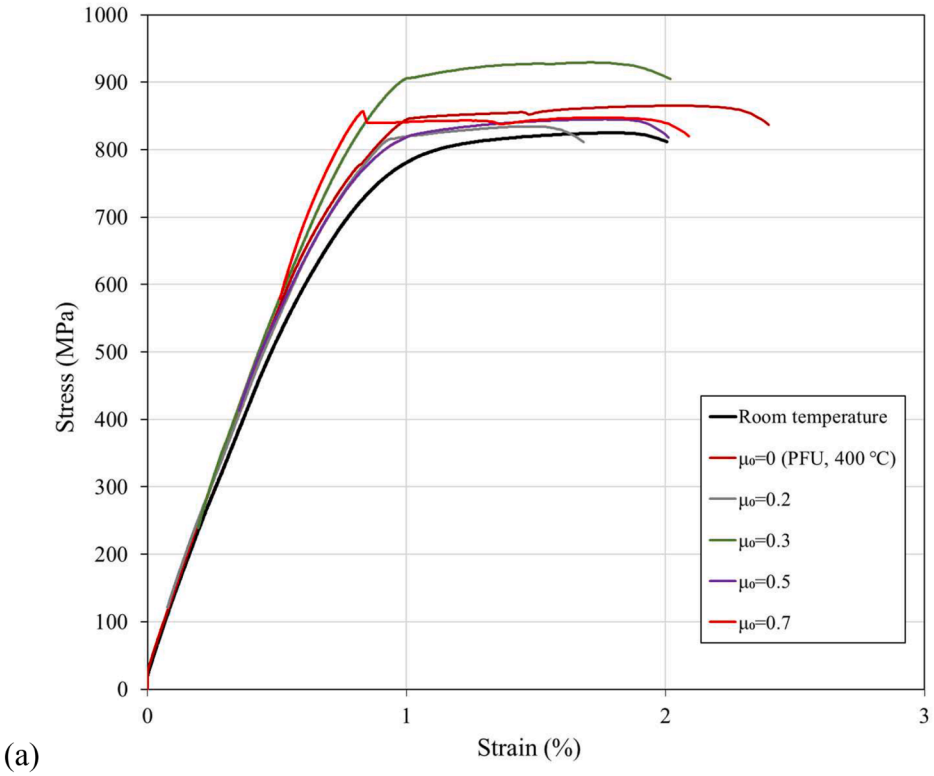


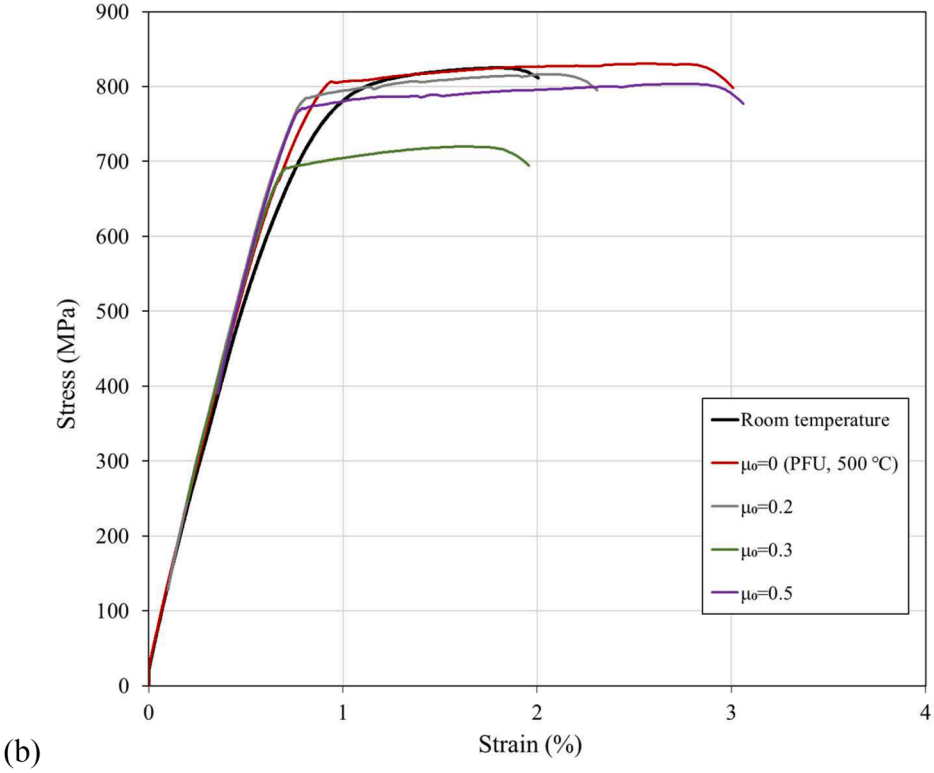
Fig. 11. Residual stress-strain curves obtained from post-fire tests (PFL) performed on S700 steel specimens cut from CHS (θ_t = 500 °C and different degrees of utilisation μ_0): (a) Set 3, (b) Set 4.

from S355 CHS (Set 6). Thus, Fig. 13 shows the residual stress-strain curves for different combinations of target temperature θ_t and degree of utilisation μ_0. As in the previous tests, the room temperature stress-strain curves and the residual stress-strain curves obtained from the PFU tests at the same target temperatures θ_t, are also plotted for reference purposes. In some of the stress-strain curves, stress fluctuations with increasing strains are caused by data sampling errors. The residual values and factors of the key mechanical properties were extracted from the curves and are reported in Tables 17 and 18.

Based on the residual factors presented in Tables 8–18, the variation trends for the key mechanical properties with the degree of utilisation μ_0 for different target temperatures θ_t are depicted in Fig. 14a–e.



(a)



(b)

Fig. 12. Residual stress-strain curves obtained from PFL tests performed on S700 steel specimens cut from CHS (Set 5) at different target temperatures and degrees of utilisation μ_0: (a) $\theta_t = 400$ °C, (b) $\theta_t = 500$ °C, (c) $\theta_t = 600$ °C.

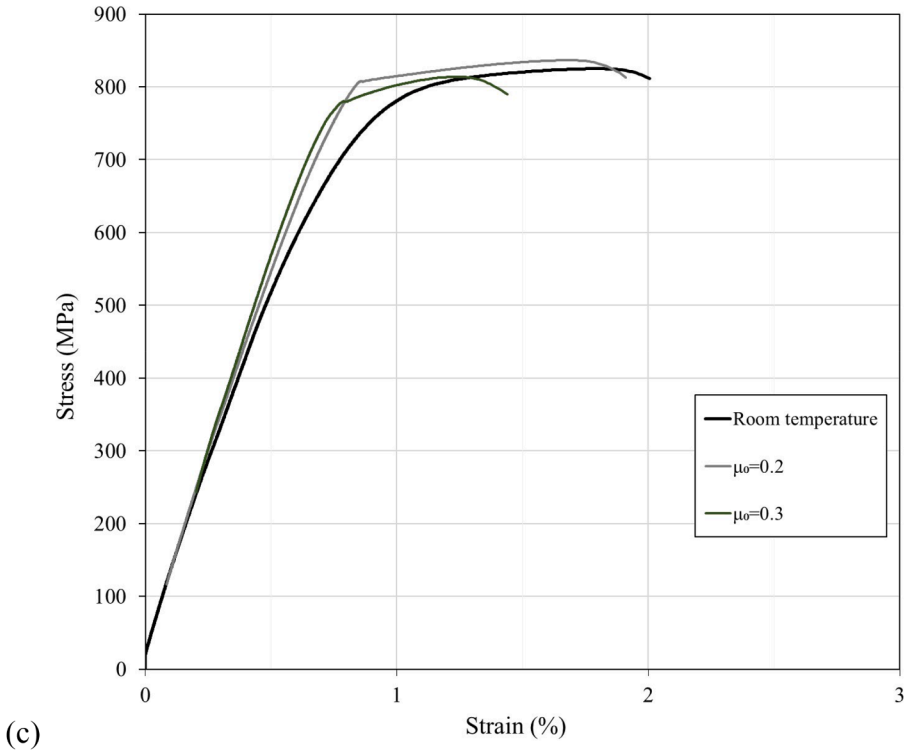


Fig. 12. (*continued*).

Table 16
Residual values and factors for key mechanical properties obtained from PFL tests on S700 steel specimens cut from CHS (Sets 3–5). Target temperatures θ_t and degrees of utilisation μ_0 are specified.

CHS Set, θ_t	μ_0	Yield strength		Tensile strength		Young's modulus	
		f_y (MPa)	$f_{y,\theta}/f_y$	f_u (MPa)	$f_{u,\theta}/f_u$	E_θ (MPa)	E_θ / E
Set 3	0	749.5	0.99	772.4	0.92	201,000	0.96
500 °C	0.2	629.9	0.83	657.5	0.78	186,000	0.89
	0.3	734.7	0.97	758.8	0.90	N/A	N/A
	0.5	734.4	0.97	764.6	0.91	217,000	1.04
	0.7	754.1	1.00	754.3	0.89	N/A	N/A
Set 4	0	730.2	1.02	757.0	0.98	204,000	0.93
500 °C	0.2	687.8	0.96	718.3	0.93	193,000	0.88
	0.3	709.0	0.99	740.1	0.96	195,000	0.89
	0.5	639.1	0.89	701.8	0.91	180,000	0.82
	0.7	737.4	1.03	760.8	0.98	213,000	0.97
Set 5	0	838.2	1.09	865.0	1.05	235,000	1.06
400 °C	0.2	818.3	1.06	834.3	1.01	199,000	0.90
	0.3	906.9	1.18	929.2	1.13	202,000	0.91
	0.5	818.6	1.06	844.9	1.02	N/A	N/A
	0.7	839.9	1.09	856.8	1.04	N/A	N/A
Set 5	0	804.7	1.05	830.4	1.01	234,000	1.06
500 °C	0.2	791.3	1.03	816.3	0.99	215,000	0.97
	0.3	697.9	0.91	719.9	0.87	161,000	0.73
	0.5	775.3	1.01	803.4	0.97	N/A	N/A
Set 5	0.2	813.3	1.06	836.5	1.01	207,000	0.94
600 °C	0.3	793.2	1.03	814.0	0.99	215,000	0.97

N/A: data not available due to measurement errors.

From Fig. 14a, it can be seen that the residual factors for yield strength $f_{y,\theta}/f_y$ are all higher than 0.8 and show no significant trend or influence relating to the degree of utilisation, though the residual factors for the S355 steel (Set 6) were consistently lower from the PFL than the PFU tests. Similarly, as shown in Fig. 14b, the residual factors for ultimate strength $f_{u,\theta}/f_u$ show no strong influence of the degree of utilisation, with the values remaining close to 0.9 for all the specimen sets. Furthermore, while the reduction factors for yield strength showed some variation with the production route and steel grade, the ultimate strength is largely insensitive to these variables.

Residual ductility is assessed by means of the residual values of ultimate strain $\varepsilon_{u,\theta}/\varepsilon_u$ and strain at fracture $\varepsilon_{f,\theta}/\varepsilon_f$, which are depicted in Fig. 14c and Fig. 14d, respectively. The specimens extracted from the S700 steel CHS (Sets 3–5) showed reduced ductility at room temperature due to the influence of cold working during production [45,48]; the results of these specimens are omitted from Fig. 14c-d, as well as Table 16. Despite the notable scatter in the results, which is often seen in measures of ductility [49], it is shown that ductility generally decreases when high temperature and tensile load are applied together, compared to the PFU results, especially at higher degrees of utilisation. Similarly, for Young's modulus (Fig. 14e), the residual values are generally lower when tensile load is applied together with temperature, relative to the PFU results, particularly at higher degrees of utilisation.

3.3.3. *Post-fire residual ductility and code provisions*

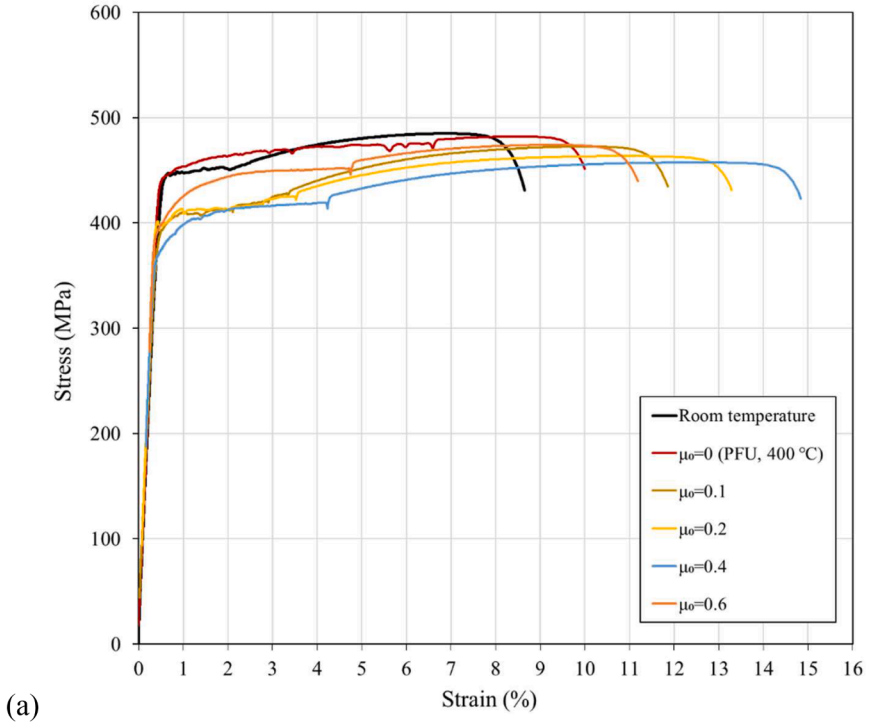
The Eurocode 3 [39] ductility requirements are, for elastic global analysis:

1. Ratio of tensile strength to yield strength: $f_u/f_y \geq 1.05$.
2. Strain at fracture $\varepsilon_f \geq 12$ % (this value is reduced to 10 % in EN 1993–1-12, which applies to S700 steels and higher [50]).

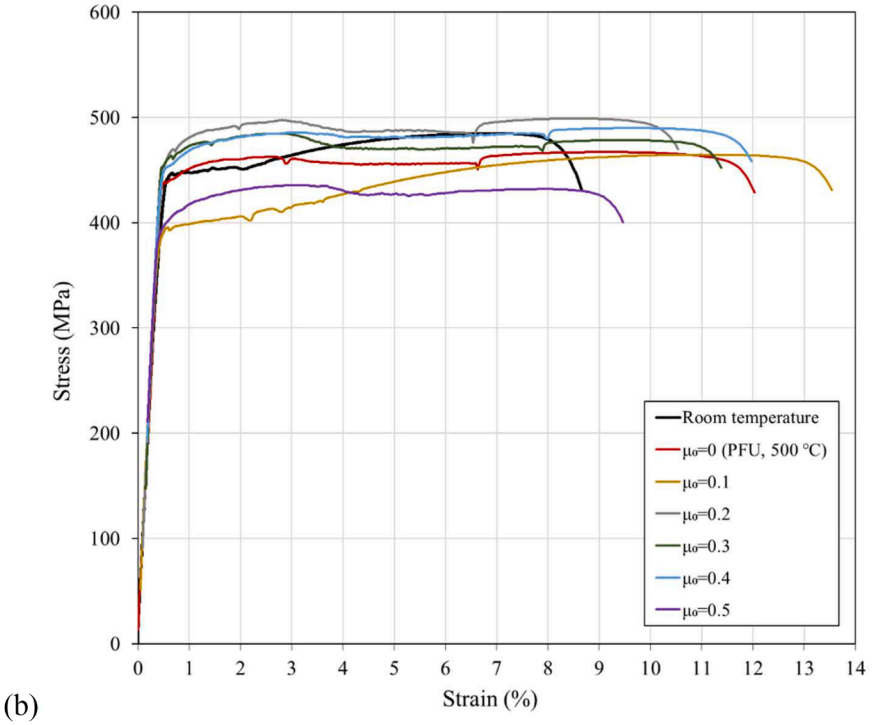
If a steel structure is to be reinstated after a fire, these ductility requirements should be met. Fig. 15 and 16 depict the application of the Eurocode 3 provisions to the residual ductility values obtained from the PFU and PFL tests, respectively. According to the graphs, differences in meeting the Eurocode 3 requirements arise if data from PFU or PFL tests are used.

Regarding the PFU tests, the requirement on the $f_{u,\theta}/f_{y,\theta}$ ratio (Fig. 15a) was met for all the target temperatures except 500 °C and 600 °C. The requirement on $\varepsilon_{f,\theta}$ (Fig. 15b) was not met for many specimens, particularly in the intermediate to high temperature range (around 700 °C to 900 °C).

For the combinations of degree of utilisation μ_0 and target



(a)



(b)

Fig. 13. Residual stress-strain curves obtained from PFL tests performed on S355 steel specimens cut from CHS (Set 6) at different degrees of utilisation μ_0: (a) $\theta_t =$ 400 °C, (b) $\theta_t =$ 500 °C.

Table 17
Residual values and factors for key mechanical properties obtained from PFL tests ($\theta_t = 400$ °C and different degrees of utilisation μ_0) on S355 steel specimens cut from CHS (Set 6).

μ_0	Yield strength		Tensile strength		Ultimate strain		Strain at fracture		Young's modulus	
	$f_{y,\theta}$ (MPa)	$f_{y,\theta}/f_y$	$f_{u,\theta}$ (MPa)	$f_{u,\theta}/f_u$	$\varepsilon_{u,\theta}$ (%)	$\varepsilon_{u,\theta}/\varepsilon_u$	$\varepsilon_{f,\theta}$ (%)	$\varepsilon_{f,\theta}/\varepsilon_f$	E_θ (MPa)	E_θ/E
0	445.4	1.00	482.1	0.99	8.36	1.24	10.67	1.16	207,000	0.99
0.1	381.0	0.85	472.6	0.97	9.85	1.46	12.51	1.36	N/A	N/A
0.2	381.0	0.85	463.5	0.96	10.53	1.56	13.96	1.52	195,000	0.93
0.4	384.0	0.86	457.5	0.94	12.47	1.85	15.49	1.68	189,000	0.91
0.6	383.3	0.86	474.2	0.98	9.09	1.35	11.90	1.29	186,000	0.89

N/A: data not available due to measurement errors.

Table 18
Residual values and factors for key mechanical properties obtained from PFL tests ($\theta_t = 500$ °C and different degrees of utilisation μ_0) on S355 steel specimens cut from CHS (Set 6).

μ_0	Yield strength		Tensile strength		Ultimate strain		Strain at fracture		Young's modulus	
	$f_{y,\theta}$ (MPa)	$f_{y,\theta}/f_y$	$f_{u,\theta}$ (MPa)	$f_{u,\theta}/f_u$	$\varepsilon_{u,\theta}$ (%)	$\varepsilon_{u,\theta}/\varepsilon_u$	$\varepsilon_{f,\theta}$ (%)	$\varepsilon_{f,\theta}/\varepsilon_f$	E_θ (MPa)	E_θ/E
0	441.0	0.99	467.0	0.96	8.80	1.31	12.74	1.38	207,000	0.99
0.1	376.4	0.84	464.7	0.96	10.98	1.63	14.26	1.55	228,000	1.09
0.2	448.6	1,00	498.9	1.03	8.33	1.24	11.36	1.23	219,000	1.05
0.3	442.7	0.99	484.6	1.00	9.87	1.47	12.18	1.32	N/A	N/A
0.4	434.3	0.97	489.9	1.01	9.36	1.39	12.76	1.39	178,000	0.85
0.5	418.7	0.94	435.6	0.90	8.45	1.26	10.16	1.10	184,000	0.88

N/A: data not available due to measurement errors.

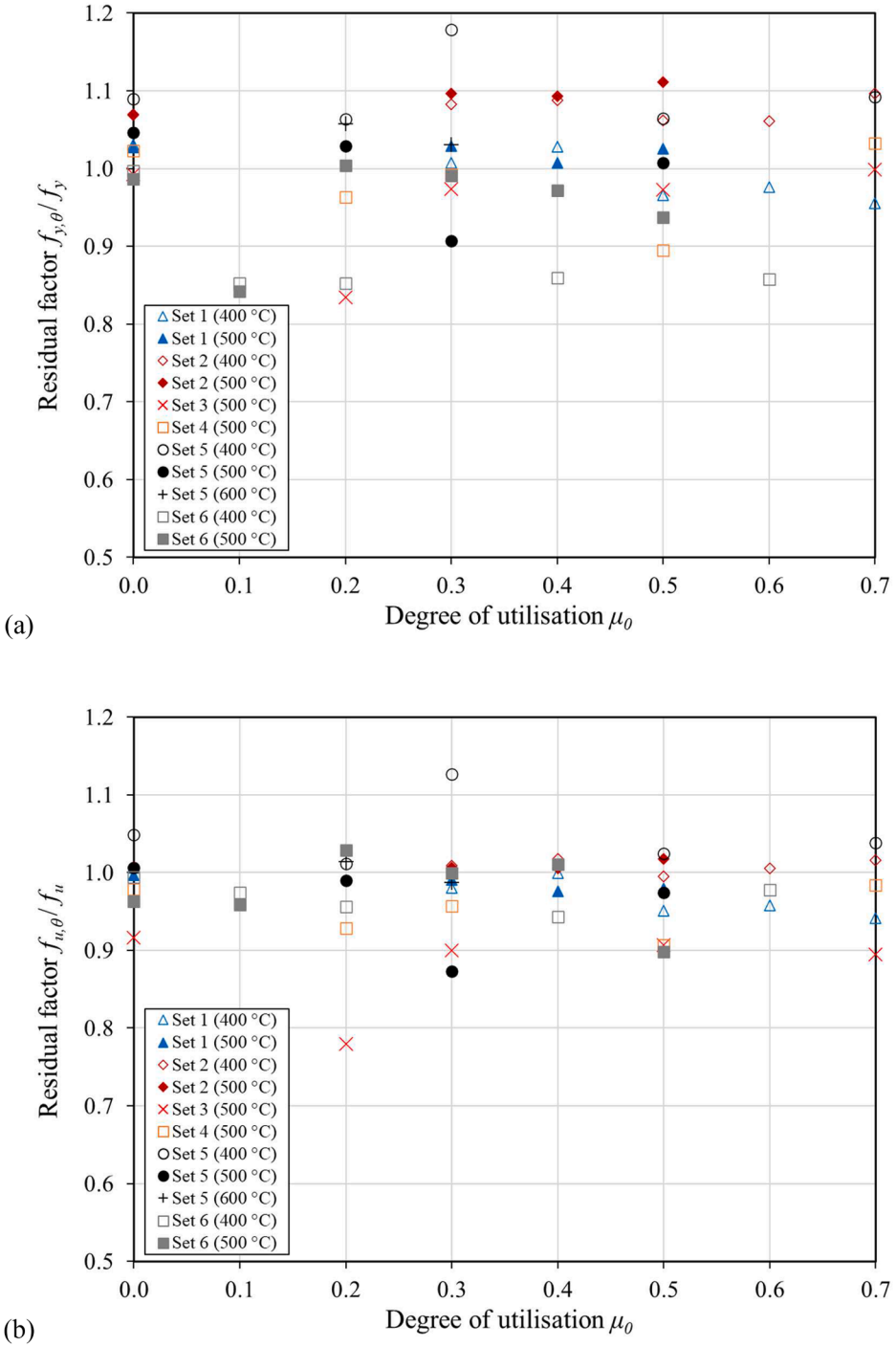
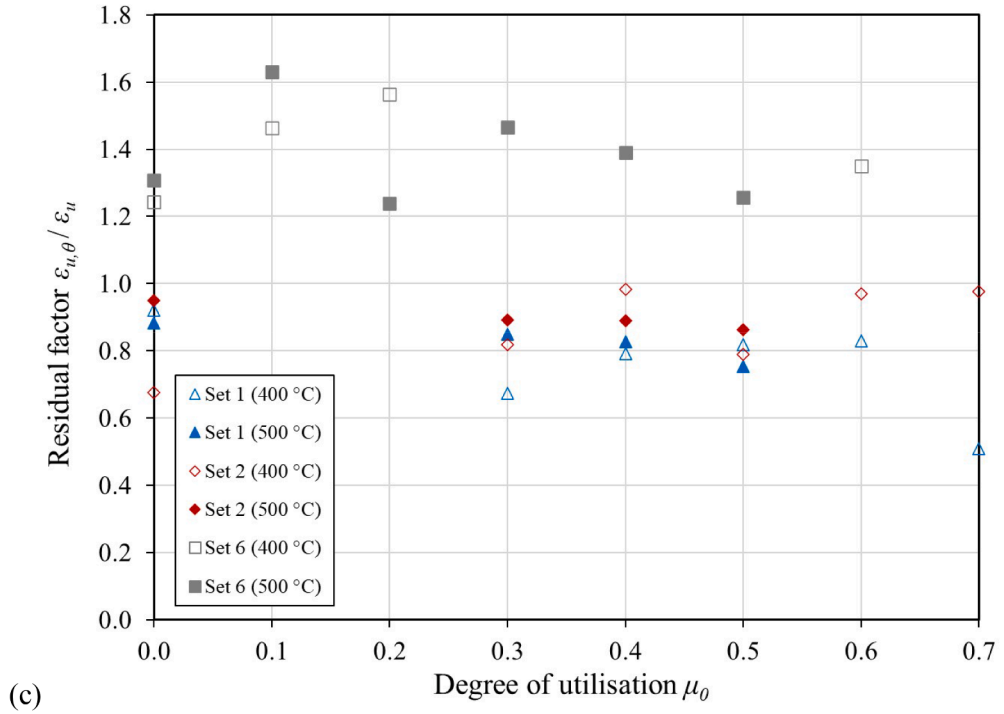


Fig. 14. Residual factors for key mechanical properties at different degrees of utilisation μ_0, obtained from post-fire tests (PFL) on Sets 1–6 at the specified target temperatures θ_t: (a) $f_{y,\theta}/f_y$, (b) $f_{u,\theta}/f_u$, (c) $\varepsilon_{u,\theta}/\varepsilon_u$, (d) $\varepsilon_{f,\theta}/\varepsilon_f$ and (e) E_θ/E.

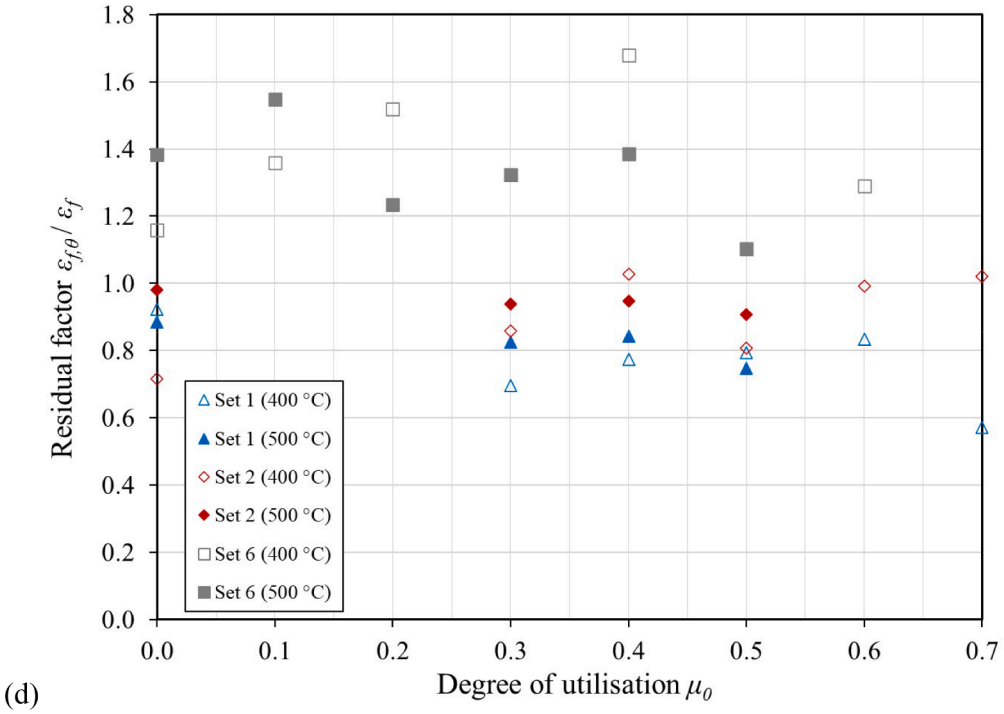
temperature θ_t considered in the PFL tests, the requirement on $f_{u,\theta}/f_{y,\theta}$ (Fig. 16a) was met for Sets 1 and 2, but not for Sets 3, 4 and 5. In contrast, for Set 6, this requirement was met for all the tested specimens. Regarding the ductility requirement on $\varepsilon_{f,\theta}$ (Fig. 16b), this was not met in some tests conducted on Set 1 specimens, although it was satisfied for all Set 2 specimens. The requirement was also not met for most specimens extracted from CHS, irrespective of the steel grade, but since the values of $\varepsilon_{f,\theta}$ were very low even at room temperature, Sets 3–6 are not presented in Fig. 16b.

4. Conclusions

An experimental campaign to evaluate the residual values of key mechanical properties (yield strength, ultimate strength, ultimate strain, strain at fracture and Young's modulus) of S700 steel specimens, extracted from S700 steel plates and CHS, exposed to temperatures between 300 °C and 1000 °C with simultaneous tensile load has been presented. The adopted experimental procedure was employed to closely simulate real fire and post-fire scenarios. For comparison, S355 steel specimens cut from CHS were also tested. Specimens underwent



(c)



(d)

Fig. 14. (*continued*).

tensile testing at room temperature, transient-state testing (to determine the *critical temperature*) and post-fire testing – unloaded (PFU) and loaded (PFL) –, involving heating to high temperatures and subsequent cooling to room temperature.

The test results showed that post-fire behaviour is influenced by the steel grade and the production route, but the degree of utilisation during heating does not generally have a strong influence. According to the findings, a threshold load during heating beyond which damage becomes critical has not been observed; also, the relative post-fire performance of HSS was found to be better than that of normal strength steel subjected to the same thermal and loading conditions. Cold-forming processes significantly reduce the ductility, irrespective of the steel grade, and residual ductility was particularly affected under specific combinations of high temperature and load. In many cases, the residual ductility did not meet the requirements of Eurocode 3. Thus, it is recommended that residual factors reflecting the steel grade and production process be incorporated into future design standards. The findings of this work support the post-fire assessment of HSS structures,

(e)

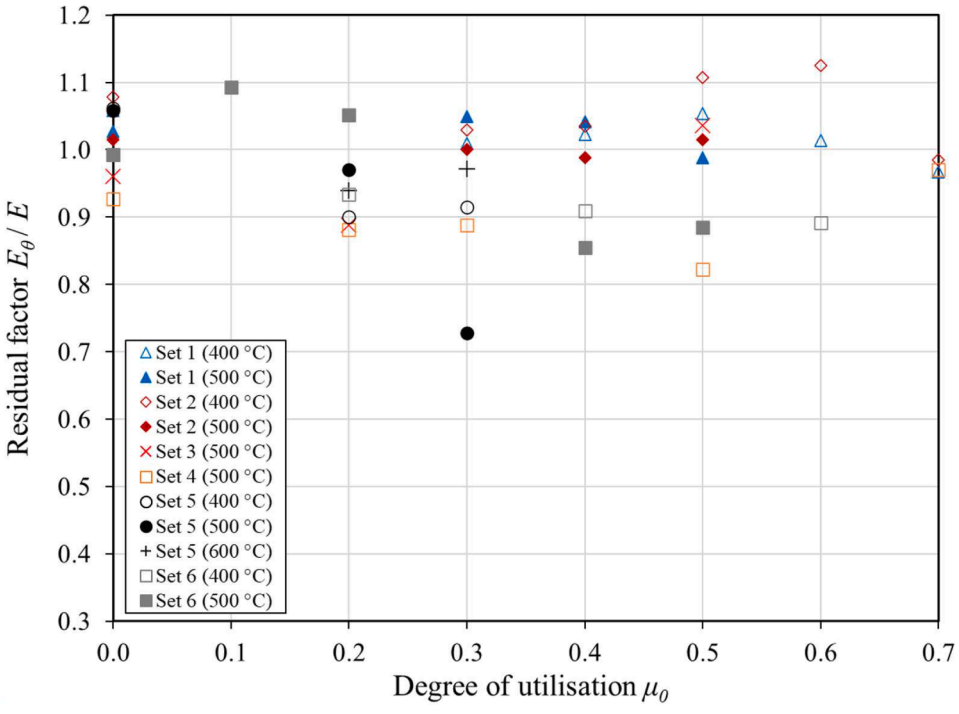


Fig. 14. (*continued*).

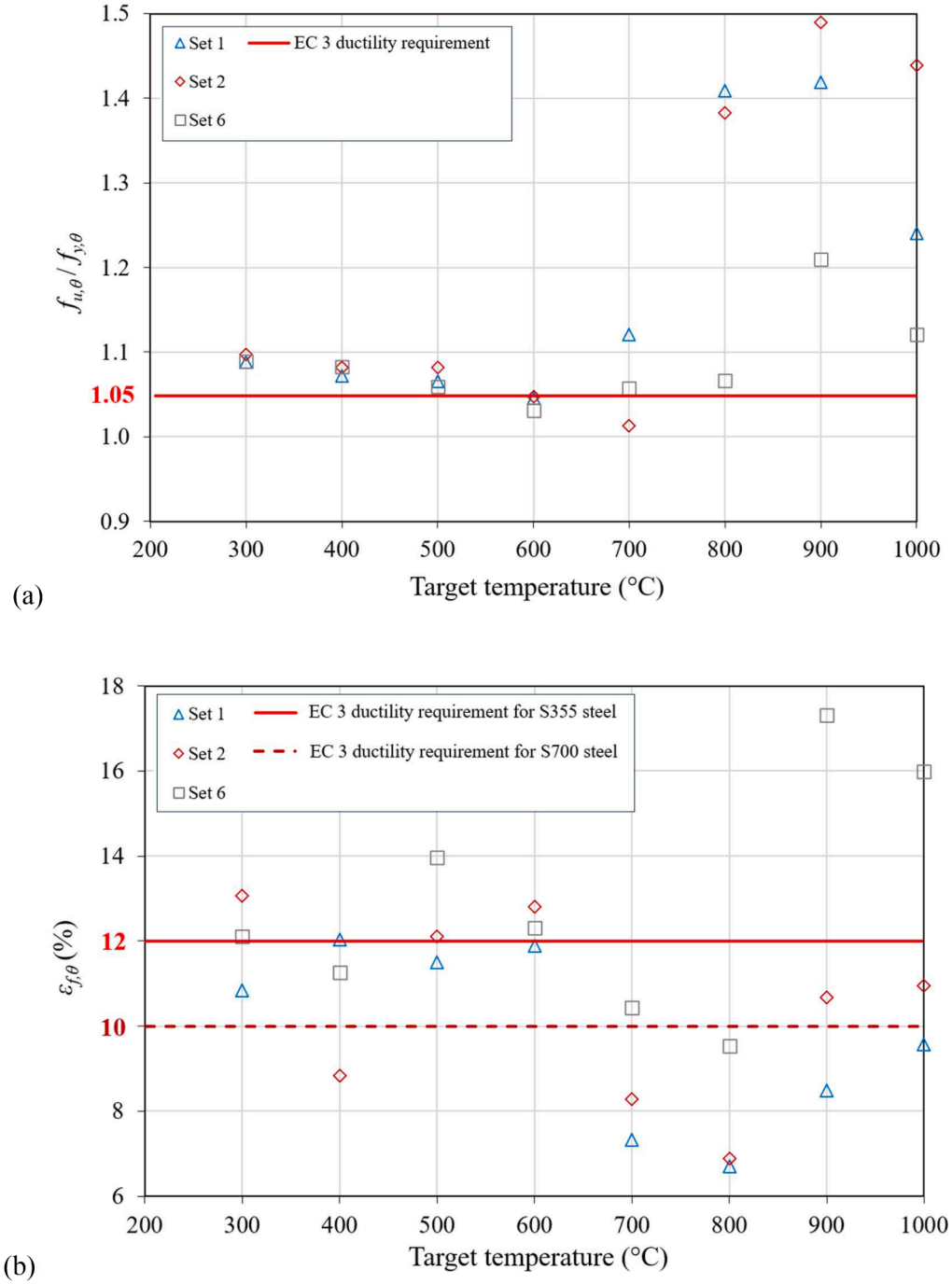


Fig. 15. Ductility indicators given by Eurocode 3 (EC3) determined from PFU tests results. (a) $f_{u,\theta}/f_{y,\theta}$ and (b) $\varepsilon_{f,\theta}$.

aiding decisions on demolition or retrofitting.

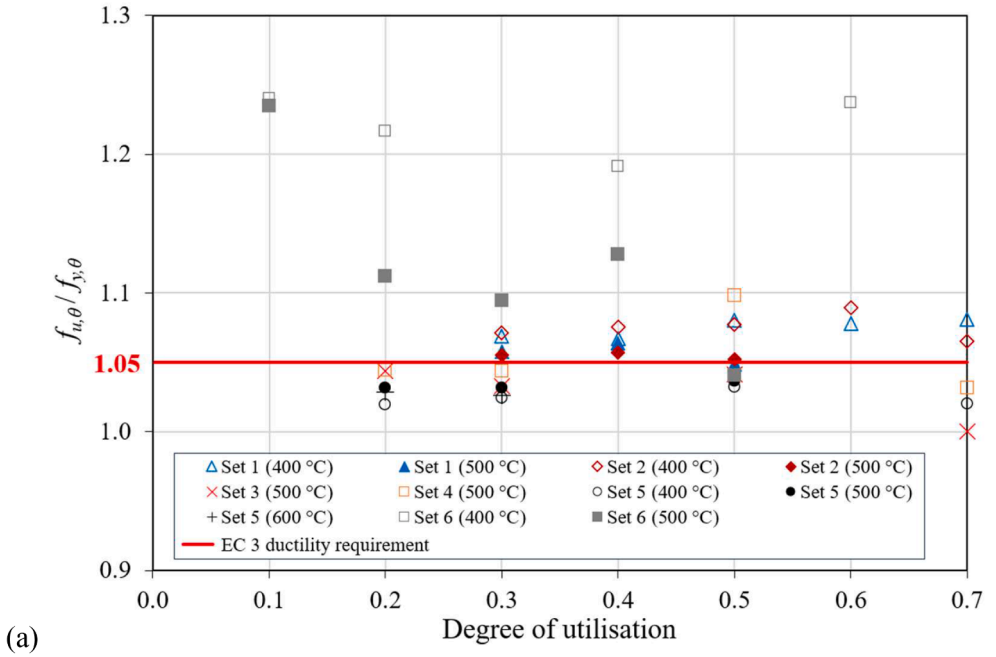
CRediT authorship contribution statement

A. Lapuebla-Ferri: Writing – review & editing, Writing – original draft, Methodology, Investigation, Conceptualization. **D. Pons:** Validation, Methodology, Investigation. **M.L. Romero:** Writing – review & editing, Validation, Supervision, Methodology, Investigation, Funding acquisition. **L. Gardner:** Writing – review & editing, Validation, Supervision, Funding acquisition.

Declaration of competing interest

The authors declare the following financial interests/personal relationships which may be considered as potential competing interests:

MANUEL L. ROMERO reports financial support was provided by State Agency Higher Council for Scientific Research. If there are other authors, they declare that they have no known competing financial interests or personal relationships that could have appeared to influence the work reported in this paper.



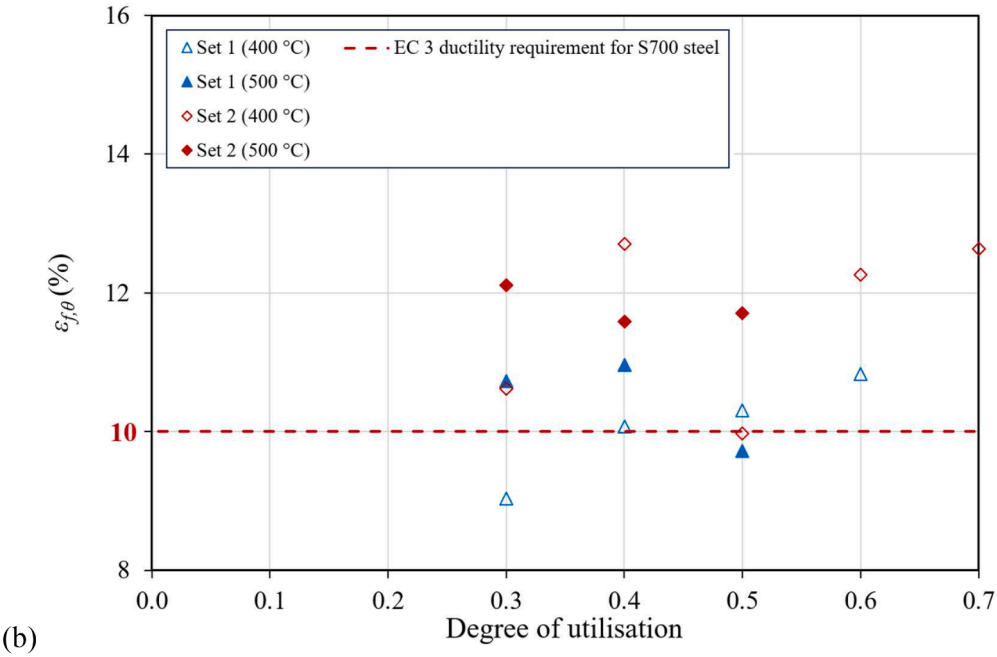


Fig 16. Ductility indicators given by Eurocode 3 (EC3) determined from PFL tests results. (a) $f_{u,\theta}/f_{y,\theta}$ and (b) $\varepsilon_{f,\theta}$.

Acknowledgements

The authors gratefully acknowledge the Spanish "Agencia Estatal de Investigación" for the help provided through the Project FIRSTIMB, carried out with a financial grant with reference TED2021-130580B-I00 funded by MCIN/AEI/ 10.13039/501100011033 and by the "European Union NextGenerationEU/PRTR". The authors want also to thank Imperial College London for the provision of the high-strength cold-formed hollow sections.

Data availability

Data will be made available on request.

References

[1] R. Bjorhovde, Development and use of high performance steel, J. Constr. Steel. Res. 60 (2004) 393–400, https://doi.org/10.1016/S0143-974X(03)00118-4.
[2] J. Wang, L. Gardner, Flexural buckling of hot-finished high-strength steel SHS and RHS columns, J. Struct. Eng. 143 (2017), https://doi.org/10.1061/(asce)st.1943-541x.0001763.
[3] X. Meng, L. Gardner, Cross-sectional behaviour of cold-formed high strength steel circular hollow sections, Thin-Walled Struct. 156 (2020), https://doi.org/10.1016/j.tws.2020.106822.
[4] G.-Q. Li, Y.-B. Wang, Behavior and Design of High-Strength Constructional Steel, Woodhead Publishing, Duxford, 2021, https://doi.org/10.1016/B978-0-08-102931-2.00001-2.
[5] E. Gehri, The fire resistance of steel structures, Fire Technol. 21 (1985) 22–33, https://doi.org/10.1007/BF01095561.

[6] L. Twilt, Strength and deformation properties of steel at elevated temperatures: some practical implications, Fire Saf. J. (1988) 13, https://doi.org/10.1016/0379-7112(88)90028-8.
[7] Y. Wang, I. Burgess, F. Wald, M. Gillie, Performance-based fire engineering of structures, 2012. https://doi.org/10.1201/b12076.
[8] M. Kucukler, Z. Xing, L. Gardner, Behaviour and design of stainless steel I-section columns in fire, J. Constr. Steel. Res. 165 (2020), https://doi.org/10.1016/j.jcsr.2019.105890.
[9] A. Espinos, L. Gardner, M.L. Romero, A. Hospitaler, Fire behaviour of concrete filled elliptical steel columns, Thin-Walled Struct. 49 (2011) 239–255, https://doi.org/10.1016/J.TWS.2010.10.008.
[10] I.R. Choi, K.S. Chung, D.H. Kim, Thermal and mechanical properties of high-strength structural steel HSA800 at elevated temperatures, Mater. Des. 63 (2014) 544–551, https://doi.org/10.1016/j.matdes.2014.06.035.
[11] S.P. Chiew, M.S. Zhao, C.K. Lee, Mechanical properties of heat-treated high strength steel under fire/post-fire conditions, J. Constr. Steel. Res. 98 (2014) 12–19, https://doi.org/10.1016/j.jcsr.2014.02.003.
[12] M. Neuenschwander, C. Scandella, M. Knobloch, M. Fontana, Modeling elevated-temperature mechanical behavior of high and ultra-high strength steels in structural fire design, Mater. Des. 136 (2017) 81–102, https://doi.org/10.1016/j.matdes.2017.09.041.
[13] D.A. Winful, K.A. Cashell, S. Afshan, A.M. Barnes, R.J. Pargeter, Elevated temperature material behaviour of high-strength steel, Proc. Inst. Civ. Eng.: Struct. Build. 170 (2017) 777–787, https://doi.org/10.1680/jstbu.16.00213.
[14] L. Huang, G.Q. Li, X.X. Wang, C. Zhang, L. Choe, M. Engelhardt, High temperature mechanical properties of high strength structural steels Q550, Q690 and Q890, Fire Technol. 54 (2018) 1609–1628, https://doi.org/10.1007/s10694-018-0760-9.
[15] W. Wang, K. Wang, V. Kodur, B. Wang, Mechanical properties of high-strength Q690 steel at elevated temperature, J. Mater. Civ. Eng. 30 (2018), https://doi.org/10.1061/(asce)mt.1943-5533.0002244.
[16] J. Jiang, W. Bao, Z.Y. Peng, Y.B. Wang, J. Liu, X.H. Dai, Experimental investigation on mechanical behaviours of TMCP high strength steel, Constr. Build. Mater. 200 (2019) 664–680, https://doi.org/10.1016/J.CONBUILDMAT.2018.12.130.
[17] G.Q. Li, L.X. Song, Mechanical properties of TMCP Q690 high strength structural steel at elevated temperatures, Fire Saf. J. 116 (2020) 103190, https://doi.org/10.1016/J.FIRESAF.2020.103190.
[18] J. Chen, B. Young, B. Uy, Behavior of high strength structural steel at elevated temperatures, J. Struct. Eng. 132 (2006) 1–7, https://doi.org/10.1061/(asce)0733-9445(2006)132:12(1948).
[19] X. Qiang, F. Bijlaard, H. Kolstein, Dependence of mechanical properties of high strength steel S690 on elevated temperatures, Constr. Build. Mater. 30 (2012) 73–79, https://doi.org/10.1016/j.conbuildmat.2011.12.018.
[20] J. Outinen, P. Tojakander, W. Lu, J. Puttonen, Material Properties of High Strength Steel in Fire, in: 7th European Conference on Steel and Composite Structures, Naples, Italy, 2014, pp. 833–834. September 10-12,2014.
[21] M.X. Xiong, J.Y.R. Liew, Experimental study to differentiate mechanical behaviours of TMCP and QT high strength steel at elevated temperatures, Constr. Build. Mater. 242 (2020) 118105, https://doi.org/10.1016/J.CONBUILDMAT.2020.118105.
[22] M.X. Xiong, J.Y.R. Liew, Mechanical properties of heat-treated high tensile structural steel at elevated temperatures, Thin-Walled Struct. 98 (2016) 169–176, https://doi.org/10.1016/J.TWS.2015.04.010.
[23] S. Shakil, W. Lu, J. Puttonen, Experimental studies on mechanical properties of S700 MC steel at elevated temperatures, Fire Saf. J. 116 (2020), https://doi.org/10.1016/j.firesaf.2020.103157.
[24] Y. Xing, W. Wang, H. Al-azzani, Assessment of thermal properties of various types of high-strength steels at elevated temperatures, Fire Saf. J. (2021) 122, https://doi.org/10.1016/j.firesaf.2021.103348.
[25] British Standards Institution (BSI), BS 5950. Structural use of steelwork in building. Part 8: code of practice for fire resistant design, London, 2003. https://shop.bsigroup.com/ProductDetail/?pid=000000000030069700 (accessed March 3, 2021).
[26] C.I. Smith, B.R. Kirby, D.G. Lapwood, K.J. Cole, A.P. Cunningham, R.R. Preston, The reinstatement of fire damaged steel framed structures, Fire Saf. J. 4 (1981), https://doi.org/10.1016/0379-7112(81)90004-7.
[27] C. Maraveas, Z. Fasoulakis, K.D. Tsavdaridis, Post-fire assessment and reinstatement of steel structures, J. Struct. Fire Eng. 8 (2017), https://doi.org/10.1108/JSFE-03-2017-0028.
[28] Y.C. Kog, Practical guide for the assessment and repair of fire-damaged concrete building structures, Pract. Period. Struct. Des. Constr. 26 (2021) 04021010, https://doi.org/10.1061/(asce)sc.1943-5576.0000570.
[29] T. Molkens, K.A. Cashell, B. Rossi, Post-fire mechanical properties of carbon steel and safety factors for the reinstatement of steel structures, Eng. Struct. 234 (2021), https://doi.org/10.1016/j.engstruct.2021.111975.
[30] X. Qiang, F.S.K. Bijlaard, H. Kolstein, Post-fire mechanical properties of high strength structural steels S460 and S690, Eng. Struct. 35 (2012) 1–10, https://doi.org/10.1016/j.engstruct.2011.11.005.
[31] C. Zhang, R. Wang, G. Song, Post-fire mechanical properties of Q460 and Q690 high strength steels after fire-fighting foam cooling, Thin-Walled Struct. 156 (2020), https://doi.org/10.1016/j.tws.2020.106983.
[32] X. Zhou, X. Xue, Y. Shi, J. Xu, Post-fire mechanical properties of Q620 high-strength steel with different cooling methods, J. Constr. Steel. Res. 180 (2021), https://doi.org/10.1016/j.jcsr.2021.106608.
[33] G.Q. Li, H. Lyu, C. Zhang, Post-fire mechanical properties of high strength Q690 structural steel, J. Constr. Steel. Res. 132 (2017) 108–116, https://doi.org/10.1016/j.jcsr.2016.12.027.
[34] H.T. Li, B. Young, Residual mechanical properties of high strength steels after exposure to fire, J. Constr. Steel. Res. 148 (2018) 562–571, https://doi.org/10.1016/j.jcsr.2018.05.028.
[35] X. Yan, Y. Xia, H.B. Blum, T. Gernay, Post-fire mechanical properties of advanced high-strength cold-formed steel alloys, Thin-Walled Struct. 159 (2021), https://doi.org/10.1016/j.tws.2020.107293.
[36] L.X. Song, G.Q. Li, Processing and cooling effects on post-fire mechanical properties of high strength structural steels, Fire Saf. J. (2021) 122, https://doi.org/10.1016/j.firesaf.2021.103346.
[37] D. Huang, L. Zhang, W. Wang, H. Mu, Test on post-fire residual mechanical properties of high strength Q690 steel considering tensile stress in fire, J. Constr. Steel. Res. 194 (2022), https://doi.org/10.1016/j.jcsr.2022.107340.
[38] A. Lapuebla-Ferri, D. Pons, M.L. Romero, Load and temperature influence on the post-fire mechanical properties of steel reinforcements, J. Constr. Steel. Res. 185 (2021), https://doi.org/10.1016/j.jcsr.2021.106866.
[39] European Committee for Standardization, EN 1993-1-1: Eurocode 3: Design of steel structures - Part 1-1: General rules and rules for buildings, 2022.
[40] Y. Liang, T. Manninen, O. Zhao, F. Walport, L. Gardner, Elevated temperature material properties of a new high-chromium austenitic stainless steel, J. Constr. Steel. Res. 152 (2019) 261–273, https://doi.org/10.1016/j.jcsr.2018.04.028.
[41] European Committee for Standardization, EN 1993-1-2: eurocode 3: design of steel structures - part 1-2: general rules - structural fire design, 2005.
[42] J. Outinen, P. Mäkeläinen, Transient state tensile test results of structural steel S355 (RAEX37-52) at elevated temperatures, Raken. Mek. 28 (1994).
[43] F. McCann, L. Gardner, S. Kirk, Elevated temperature material properties of cold-formed steel hollow sections, Thin-Walled Struct. 90 (2015) 84–94, https://doi.org/10.1016/j.tws.2015.01.007.
[44] J.L. Ma, T.M. Chan, B. Young, Material properties and residual stresses of cold-formed high strength steel hollow sections, J. Constr. Steel. Res. 109 (2015) 152–165, https://doi.org/10.1016/j.jcsr.2015.02.006.
[45] B. Rossi, S. Afshan, L. Gardner, Strength enhancements in cold-formed structural sections — Part II: predictive models, J. Constr. Steel. Res. 83 (2013), https://doi.org/10.1016/j.jcsr.2012.12.007.
[46] P. Kyvelou, L. Gardner, D.A. Nethercot, Finite element modelling of composite cold-formed steel flooring systems, Eng. Struct. 158 (2018) 28–42, https://doi.org/10.1016/j.engstruct.2017.12.024.
[47] Z. Tao, X.Q. Wang, B. Uy, Stress-strain curves of structural and reinforcing steels after exposure to elevated temperatures, J. Mater. Civ. Eng. 25 (2013) 1306–1316, https://doi.org/10.1061/(ASCE)MT.1943-5533.0000676.
[48] S. Afshan, B. Rossi, L. Gardner, Strength enhancements in cold-formed structural sections — part I: material testing, J. Constr. Steel. Res. 83 (2013), https://doi.org/10.1016/j.jcsr.2012.12.008.
[49] L.N. Dissanayake, F. Walport, X. Yun, L. Gardner, Unified stress-strain models for normal and high strength steels, Constr. Build. Mater. 459 (2025) 139616, https://doi.org/10.1016/J.CONBUILDMAT.2024.139616.
[50] European Committee for Standardization, prEN 1993-1-12:2024. Eurocode 3: design of steel structures - part 1-12: additional rules for steel grades up to S960, 2024.